

République Algérienne Démocratique et Populaire  
Ministère de L'enseignement Supérieur et de la Recherche Scientifique  
Université de Bejaia

## **MEMOIRE**

pour obtenir le grade de  
**Magister en électrotechnique**  
**Option : système électroénergétique**  
présenté et soutenu publiquement  
par

**OUHAB Abdelwahab**

Titre :

**Dye Sensitized Solar Cell  
Concepts and Realization**

Jury

Dr.SAMAH Madani	(Université de Bejaia)	Directeur de thèse
Dr.AMARDJIA Hania	(Université de Setif)	Co-directeur de thèse
M.KHELFAOUI Youcef	(Université de Bejaia)	Président du jury
M.MOUSSI Abderrahmane	(UDTS Alger)	Examineur
M.BOUKHALFA Yaici	Responsable projet(Cevital )	Invité

*Université de Bejaia 2008*

# Acknowledgements

First of all, I gratefully acknowledge Mr. Isaad Rebrab - PDG of Cevital - who immediately accepted to finance this project and gave me the opportunity to make the experimental part of this subject at Lyon 1 University (France).

I also gratefully acknowledge my two promoters Dr. Samah Madani and Dr. Amardjia Hania of the university (Ferhat Abbas of Sétif) who gave me the opportunity to work on this subject and for the help they gave me all along this work.

I would like to thank Prof. Jean Claude Plenet the manager of PMCN laboratory at Lyon 1 University (France), for the opportunity he has given to me by receiving me in his Laboratory and for the facility he gave me to achieve my work.

A special thank to the staff of the BLS language school In particular : Ms. Yasmine my teacher of english, Mr. Yacine and Ms. Souade the school managers, for facilitating me to begin my formation in the school and for the help they gave me all along my formation.

I would like to thank who helped me in my experimental results:

- Prof. Jean-Plettier from laboratory : MATEIS for having done XRD spectrum of  $TiO_2$
- Prof. Mustapha Lemiti from laboratory (LPI) national institute of applied sciences INSA Lyon for the measurements of  $TiO_2$  layer thickness.
- Mr. Moussi Abderrahmane and Mr. Dahmani Abdelouahab from development unit of silicium technology(UTDS Alger) for their help in IPCI measurements which I made in their laboratory.
- Mr. Ouennoughi from (University Ferhat Abbas of Sétif, faculté des sciences département de physique) for their help in currentvoltage measurements which I made in his laboratory.

I would like to acknowledge Mr. Rezki Djamel the Energies Manager at Cevital-Bejaia who followed me during all the period of this work with his counsils and his encouragements. Many thanks to all Cevital managers who gave me help in this project These are in particular:

- Mr. Hamga Youcef the Informatique Manager.
- Mr. Morsli Mohamad the General Manager of Cevielec.
- Mr.Boukhalfa Yaici the Renewable Energies Project Manager.

I acknowledge the members of my jury, who have invested time to read and judge my report.

# Contents

<b>Introduction</b>	<b>6</b>
<b>1 History and state of the art</b>	<b>9</b>
1.1 Energy consumption in the world . . . . .	9
1.2 Renewable energies . . . . .	12
1.2.1 Solar energy . . . . .	12
1.2.2 Hydroelectric power . . . . .	13
1.2.3 Wind energy . . . . .	13
1.2.4 Biomass energy . . . . .	14
1.2.5 Geothermal energy . . . . .	15
1.2.6 Ocean energy . . . . .	15
1.3 Photovoltaics - A brief history . . . . .	15
1.3.1 Classical systems . . . . .	15
1.3.2 Dye-Sensitized Solar Cells . . . . .	18
1.4 References of Chapter 1 . . . . .	20
<b>2 Photovoltaic technologies</b>	<b>21</b>
2.1 Silicon . . . . .	21
2.1.1 Si (single-crystal) . . . . .	22
2.1.2 Si (multicrystalline) . . . . .	23
2.1.3 Si (thin-film transfer) . . . . .	24
2.2 III-V cells . . . . .	25
2.3 Polycrystalline thin film . . . . .	27
2.4 Amorphous silicon . . . . .	28
2.5 Photoelectrochemical cells . . . . .	30
2.5.1 Nanocrystalline Dye-Sensitized Solar Cells . . . . .	30
2.6 Multijunction cells . . . . .	30
2.7 References of Chapter 2 . . . . .	33
<b>3 Dye-Sensitized Solar Cell</b>	<b>34</b>
3.1 Advantageous of the Dye-Sensitized Solar Cell . . . . .	34
3.2 Dye-Sensitized Solar Cell components . . . . .	34
3.3 Dye-Sensitized Solar Cell Fabrication . . . . .	35

3.4	Operating Principles of the Dye-Sensitized Solar Cell . . . . .	36
3.5	Electron transfer dynamics . . . . .	37
3.6	Semiconductor Films . . . . .	38
3.7	Importance of morphologie of $TiO_2$ films . . . . .	38
3.8	Requirements of the Sensitizers . . . . .	39
3.9	The general structure of the dye . . . . .	40
3.10	Electrolyte . . . . .	42
3.11	Solid state Dye-Sensitized Solar Cells . . . . .	42
3.12	Counter electrodes . . . . .	44
3.13	References of Chapter 3 . . . . .	45
<b>4</b>	<b>General properties of titanium dioxide</b>	<b>48</b>
4.1	$TiO_2$ crystal structures . . . . .	48
4.2	Semiconductor properties . . . . .	49
4.3	References of Chapter 4 . . . . .	53
<b>5</b>	<b>Experimental</b>	<b>55</b>
5.1	preparation . . . . .	55
5.1.1	Components of DSSC . . . . .	55
5.1.2	Materials . . . . .	55
5.1.3	TCO Substrates . . . . .	56
5.1.4	Choice of the TCO . . . . .	56
5.1.5	Deposited of $TiO_2$ electrodes . . . . .	57
5.1.6	ruthenium sensitizer . . . . .	57
5.1.7	Preparation of counter Pt-electrodes . . . . .	57
5.1.8	Electrolyte . . . . .	58
5.1.9	DSSC assemblage . . . . .	58
5.2	Characterizations methods . . . . .	58
5.2.1	X-Ray Diffraction . . . . .	58
5.2.2	Photovoltaic characterisation . . . . .	60
5.3	Results and discussion . . . . .	63
5.3.1	X-Ray Diffraction . . . . .	63
5.3.2	current-voltage measurements . . . . .	63
5.3.3	The measurement of incident photon-to-current conversion	64
5.4	References of Chapter 5 . . . . .	67
	<b>CONCLUSIONS</b>	<b>68</b>

# Introduction

The conversion of sunlight into electricity is a clean, abundant and renewable energy source. The efficiency of conventional solar cells made from inorganic materials reached up to 24% [1], using very expensive materials of high purity and energy intensive processing techniques.

Photovoltaic devices are based on the concept of charge separation at an interface of two materials of different conduction mechanism. To date this field has been dominated by solid-state junction devices, usually made of silicon, and profiting from the experience and material availability resulting from the semiconductor industry. The dominance of the photovoltaic field by inorganic solid-state junction devices is now being challenged by the emergence of a third generation of cells, based, for example, on nanocrystalline and conducting polymer films. These offer the prospective of very low cost fabrication and present attractive features that facilitate market entry.

Contrary to expectation, devices based on interpenetrating networks of mesoscopic semiconductors have shown strikingly high conversion efficiencies, which compete with those of conventional devices. The prototype of this family of devices is the Dye-Sensitized Solar Cell, which realizes the optical absorption and the charge separation processes by the association of a sensitizer as light-absorbing material with a wide band gap semiconductor of nanocrystalline morphology [2].

In this work we will mainly focus on the concepts and the dynamic preparation of nanoporous  $TiO_2$  films for the fabrication of Dye-Sensitized Solar Cell.

The present work is described as follows.

Chapter 1 : gives some statistics about energy consumption rate in the world and describes sources of renewable energies depend either directly or indirectly from the sun's radiation. Then gives a brief history review of photovoltaics.

Chapter 2 : will focus on existing and newly developed photovoltaic tech-

nologies. One attractive new type of photovoltaic system that mimic natural photosynthesis.

Chapter 3 : This chapter describes the different components of the Dye-Sensitized Solar Cell (DSSC). The role and the properties of the different constituent components of the device .

Chapter 4 : starts with a description of the different polymorphs of titanium dioxide and the properties of  $TiO_2$  as reported in the literature are summarized. Then, a short reminder the properties of semiconductors are presented.

Chapter 5 : In the initial part of this chapter is discussed the materials and technique used for the preparation of Dye-Sensitized Solar Cell (DSSC). The second part of this chapter describes the measurements have been made for characterising the cell.

Finally, in the conclusion the results obtained are summarized .

## References

- [1] M. Green, *Progr. Photovolt.* 9 (2001) 123.
- [2] (a) B. O'Regan, M. Gratzel, *Nature* 335 (1991) 737;  
(b) M. Gratzel, *Nature* 414 (2001) 338-344.

# Chapter 1

## History and state of the art

### 1.1 Energy consumption in the world

For many thousand of years till about three hundred years ago, mankind used exclusively renewable energy sources (with a minor exploitation of coal). Wood was used for heating, animals were used for transportation, and wind and water supplied mechanical energy. During the 19th century, the industrial revolution brought new machines and new energetic needs; coal was found to satisfy the increasing demand of energy. The early 20th century saw the first exploitation of petroleum, natural gas and later, nuclear energy as energy sources to cover the continuously growing demand. Nowadays, fossil energies cover 95% of the total energy demand worldwide, which exceeds 105 TWh per year.

Global energy consumption draws from six primary sources: 44% petroleum, 26% natural gas, 25% coal, 2.5% hydroelectric power, 2.4% nuclear power, and 0.2% non-hydro renewable energy [1]. Between 1980 and 2001, worldwide consumption of petroleum, coal, and natural gas increased by 22, 27, and 71% respectively.

Following the projected energy needs, this will increase by nearly 50% in the 25 next years. About 30% of the primary energy is converted to electricity either in the course of initial harvesting (as for hydroelectric, wind, solar and geothermal) or by combustion (as for fossil, and biomass); about 75% of the primary energy arrives, in one form or the other, at the consumer.

As estimates of non-commercial energy use are incomplete and unreliable, the above estimates do not include nonmarket wood used as fuel and farm residues that are prevalent in many countries. The international energy agency (IEA) suggests that biomass still provides on average one-third of the energy needs in Africa, Asia, and Latin America, and as much as 80 to 90% in the poorest countries of these regions.

While the average yearly energy consumption per capita in developing countries is about 10 MWh (with about 1 MWh in the poorest !), the yearly consumption in Europe amounts to about 50 MWh and in the USA to 90 MWh per capita. The energy consumption can be classified by sectors, as shown in Figure 1.1; the most important ones are residential, transportation, and industry. The importance of these sectors differs between developing and developed countries. For example, transportation in the developed countries accounts for 35% of the total energy consumption, whilst in the developing ones roughly 18%.

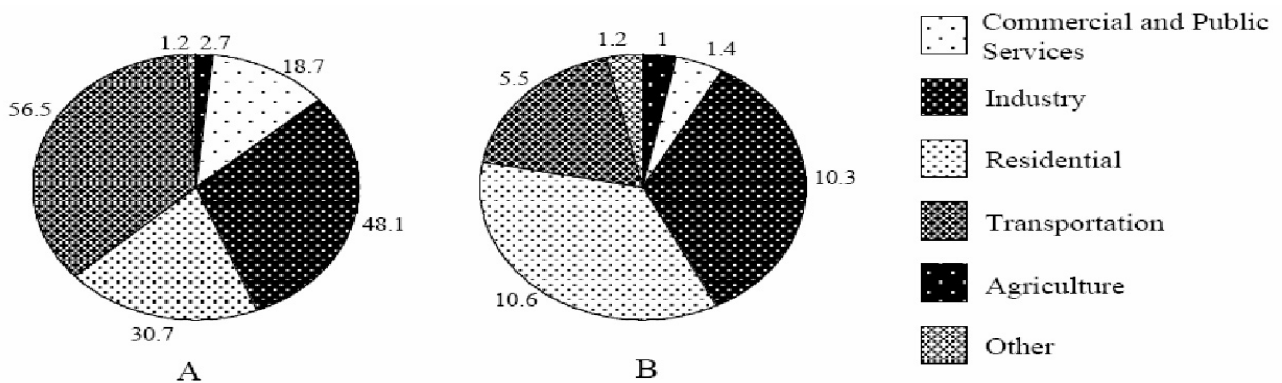


Figure 1.1: Per-capita energy consumption by sectoral end use in (A) the developed world and (B) the developing world (in gigajoules)

Although estimates vary, economically recoverable fossil fuel reserves include almost one trillion tons of coal, more than one trillion barrels of petroleum, and over 150 trillion cubic meter of natural gas. Roughly 3 million tons of uranium reserves are known. Annually, the world consumption of coal is about 0.5% of the reserves, of natural gas around 1.6% of reserves, whereas oil almost 3% of reserves, and nuclear electricity generation consumed the equivalent of 2% of uranium reserves.

Large fossil fuel reserves are concentrated in a small number of countries, with a large number of developing countries having no reserves at all. Many energy-lacking countries have become highly developed through sufficient access to international energy markets. Conversely, some countries possess substantial reserves but remain rather poor. This shows that the possession of reserves is not a sufficient condition to a country's development unless there is an adequate economic system able to transform these energy resources into general social wealth.

Major changes in the global climate must be expected as a consequence of the carbon dioxide emissions from burning fossil fuels, which at present are of

the order of 6.6 billion tons [1] carbon equivalent and still rising. These emissions lead to an enhancement of the atmospheric  $CO_2$  concentration, passing from 280 ppm in 1850 to nearly 370 ppm in 2000 [2] and to an increase in global mean temperature of nearly  $1^\circ C$ .

Fossil fuel consumption also results, to a lesser extent, in the emission of other greenhouse gases (GHG's), such as carbon monoxide, methane, and volatile organic compounds, and the rising ocean temperature increases evaporation and hence the water vapour content in the atmosphere. The Intergovernmental Panel on Climate Change (IPCC) predicts, based on climate models, that continued emissions of anthropogenic GHG's will result in not only increasing mean temperatures but also in more frequent extreme climate events which will have significant consequences for ecosystems but also for human activities, including the flooding of low-lying land due to the thermal expansion of the ocean. The United Nations, recognizing these threats, have organized the conclusion, at the Conference in Rio in 1992, of the Framework Convention on Climate Change, which has been ratified by all participating countries. After 10 years of negotiations, targets numbers for the reduction of  $CO_2$  emissions for countries or groups of countries have been defined at the 2002 Conference at Kyoto, which however, have not yet been ratified by the main  $CO_2$  emitter, the USA and, several other countries.

While nuclear fusion is still a subject under development and will, in the opinion of experts, take the order of 50 years to reach a state of useful energy production, nuclear fission is being exploited in approx. 430 reactor units worldwide with a total capacity of about 350 GW (electr.). The construction of new reactors continues to meet at present strong opposition by part of the population because of the fear of nuclear run-away. However the run-away risk after several thousands years of integrated (over all existing reactors) run-time is, very small compared to the risks taken by the individual in every-day life (e.g. in road traffic).

The duration of the resources of uranium could be considerably extended by reprocessing of the used fuel elements.

The radioactive wastes occurring from this energy production give rise to a storage problem, as the decomposition of those takes several billion of years. Nevertheless the amount of wastes are small (15 m<sup>3</sup> per year for a 1 GW installation) and the estimate cost for long-time and safe storage is roughly 10% of the total supply cost of the fission material.

## 1.2 Renewable energies

Planet Earth receives from the sun an almost constant flux of radiation, which with clear sky and dry air amounts to about  $1\text{kW}/\text{m}^2$ . All sources of renewable energies depend either directly or indirectly from the sun's radiation. Although of lesser importance, geothermal energy sources (which derive their energy from the nuclear decay in the earth) and tidal energy (due to the gravitational forces between earth and moon) should also be practically inexhaustible.

Sunlight, or solar energy, can be used directly for heating, lighting, generating electricity and many other applications. Indirectly, sun's heat also creates winds, whose energy is used to generate electricity by wind turbines. Sunlight causes plants to grow. The organic matter composing those plants is known as biomass. Biomass can be used to produce electricity, transportation fuels for example. On the other hand, geothermal energy traps the Earth's internal heat and can be used for a large variety of applications such as building heating and electricity production. Ocean energy can under favourable conditions be used for the production of electricity.

### 1.2.1 Solar energy

A large variety of techniques are available or under development to benefit from the solar energy, including photovoltaic systems, concentrating solar power, passive solar systems, solar hot water, and solar process heat.

Photovoltaic solar cells are used to directly convert light energy into electricity, and have been available for many years; major applications like solar panels on satellites made them famous, and smaller uses like calculator or watch energy supply, known by everyone. They are based on the photovoltaic effect, which allows the conversion of light (photons) to electricity (electrons).

Concentrating solar power can be achieved by several types of systems, which share a feature that the incident solar radiation is concentrated onto a small surface. A fluid (often oil) flows through this small surface to be heated; this heat is then used to produce steam, which drives turbines, generators then create electricity. The different types of plants are shown on Figure 1.2. Parabolic trough reflector systems totalling about 350 MW are already in use in the United States and development of all three types are under way in Europe.

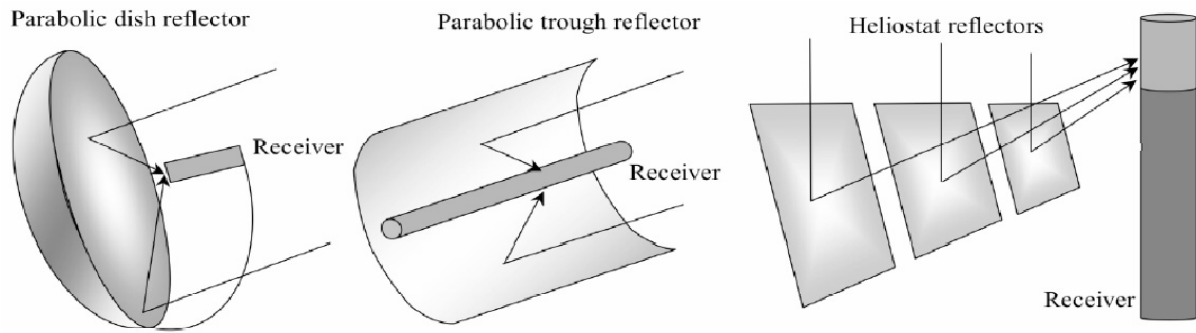


Figure 1.2: Three main types of solar concentrating collector plants

Solar chimney technology is created when the sun's radiation is used to heat a large body of air, which is then forced to move as a hot wind through turbines to generate electricity. A huge project is in development in northern Australia; a 7 km diameter transparent roof with at its center a tower (170 m  $\times$  1000 m) should reach a maximal power of 200 MW. Passive heating of buildings can be achieved by installing large windows on the south side as they receive most sunlight. More efficiently, a sunspace (similar to a greenhouse) is built on the south side of a building with ventilation allowing the heat to circulate into the building.

### 1.2.2 Hydroelectric power

Water wheels have been driving mills and heavy tools for many centuries. Currently, hydroelectric power is the world's largest renewable source of electricity, accounting for about 15% of the world's electricity. Even if hydroelectric energy does not release any standard atmospheric pollutants, the impact of this technology on the environment is not negligible. The most obvious one is the flooding of large areas of land, much of it previously forested or used for agriculture. Damming a river alters the amount and quality of water in the river downstream of the dam, as well as preventing fish from migrating upstream to spawn; on the other hand, it protects land downstream against flooding.

### 1.2.3 Wind energy

Again, wind energy has been used for many centuries for the pumping of water and grinding grain, using windmills. Some 200,000 windmills could be counted in Europe in the 18th century. Their modern equivalent, called wind turbines, use wind energy to generate electricity. Different types of turbines exist, the most common ones are the horizontal axis turbines which are mounted on towers, reaching 80 meters height, designed to take advantage of faster and more

stable winds. The biggest units can produce up to 5 MW. Vertical axis turbines also exist but are not in wide use.

According to the American Wind Energy Association (AWEA) [2] at the end of 2002 the total production capacity reached over 31000 MW worldwide; on a percentage basis wind is the fastest growing energy source with an annual increase of over 30% per year in the five last years. 75% of the total production takes place in Europe: Germany, Denmark, Spain, and the U.K. are the principal producers (89 %). In Denmark, wind energy meets 20% of the country's electricity needs, in Germany 4.5% of electricity is generated using wind.

### 1.2.4 Biomass energy

Mankind has been using biomass energy for thousand of years, since people started burning wood to cook food or to keep warm. Biomass refers to any plant-derived matter available on a renewable basis, including dedicated energy crops and trees, agricultural food and feed crops, agricultural crop wastes and residues, wood wastes and residues, aquatic plants, animal wastes, municipal wastes, and other waste materials. Bioenergy is used to produce a large array of products like electricity, solid, liquid and gaseous fuels, heat, and chemicals. Of course by burning organic materials  $CO_2$  is released in the atmosphere, but the same amount of  $CO_2$  is actually removed when new plants are growing. The net emission of  $CO_2$  will be zero as long as plants continue to be replenished for biomass energy purposes. Biomass can be directly converted into liquid fuels, mainly ethanol and biodiesel to be used for transportation needs. Biopower is the use of biomass to generate electricity. Most of the biopower plants use direct burning of the biomass for steam production, to drive a generator to produce electricity. Biobased products include green chemicals, renewable plastics, natural fibers and natural structural materials. Many of these products can replace products and materials traditionally derived from petrochemicals, but new and improved processing technologies will be required.

Bioenergy accounts for 3% of the primary energy production in the United-States, being in second rank after hydropower in renewable primary energy production. In Europe, wood accounts for more than half of the renewable primary energy production, excluding hydropower. Great efforts are made to increase the production of biogas and biofuels, an annual growth of 30% is expected until 2010 [3].

### 1.2.5 Geothermal energy

Geothermal energy uses the heat of earth for the production of electricity, for the direct use of the hot water for heating, and for geothermal heat pumps, which are used to heat and cool buildings. Geothermal energy is not easily accessible all over the world; however some countries take great advantage of this energy. In Iceland geothermal energy provides half of the total energy consumption, the other half being provided by hydropower; it is principally used for space heating (85% of the households).

### 1.2.6 Ocean energy

Ocean energy draws on energy of the ocean waves, currents and of tides. One estimates that the power of the waves breaking on the world's coastlines is around  $2 \times 10^6$  MW, but it is very expensive to collect. A dam is typically used to convert tidal energy into electricity by forcing the water through turbines, activating a generator.

The largest plant worldwide is located in France on the river La Rance. Its power production is 240 MW and has been operating since 1966. Recently, tests have begun to extract some electricity from strong ocean currents by turbine/generator sets submerged at a certain depth.

A great amount of thermal energy is stored in the world's oceans, which daily receive heat from the sun equal to the thermal energy contained in 250 billion barrels of oil.

The useful temperature difference is however too small for converting some of this enormous amount of energy into electricity.

## 1.3 Photovoltaics - A brief history

### 1.3.1 Classical systems<sup>1</sup>

**1839 - 1899 : Discovery of basic phenomena and properties of photovoltaic materials**

A physical phenomenon allowing light to electricity conversion the photovoltaic effect was discovered in 1839 by the French physicist Alexandre Edmond Bec-

---

<sup>1</sup>Adapted from [www.pvresources.com](http://www.pvresources.com) ©Denis Lenardic 2001-2003.

querel.[4] Experimenting with metal electrodes and electrolyte he discovered that the conductance rises with illumination.

Willoughby Smith discovered the photovoltaic effect in selenium in 1873.[5] In 1876, with his student R. E. Day, William G. Adams discovered that illuminating a junction between selenium and platinum also has a photovoltaic effect.[6] These two discoveries were the foundation for the first selenium solar cell construction, which was built in 1877. Charles Fritts first described them in detail in 1883.

### **1900 - 1949 : Theoretical explanation of the photovoltaic effect and the first solar cells**

The author of the most comprehensive theoretical work about the photovoltaic effect was Albert Einstein, who described the phenomenon in 1904.[7] For his theoretical explanation he was awarded a Nobel Prize in 1921. Einstein's theoretical explanation was experimentally proved by Robert Millikan in 1916.

In 1918, a Polish scientist Czochralski discovered a method for monocrystalline silicon production, which enabled monocrystalline solar cells production.[8] The first silicon monocrystalline solar cell was constructed in 1941.

In 1932, the photovoltaic effect in cadmium-selenide was observed . Nowadays, CdS belongs among important materials for solar cells production.

### **1950 - 1969 : Intensive space research**

In 1951, the first germanium solar cells have been made. Dr. Dan Trivich of Wayne State University has made some theoretical calculations on solar cell efficiency with different materials in 1953. In 1954, the RCA Laboratories published a report on a CdS photovoltaic effect. The Bell Laboratories published the results of a solar cell operation with 4.5% efficiency. The efficiency was increased to 6% within a few months.

In 1955, the development of a satellite energy supply using solar cells was initiated the material. Hoffman Electronics-Semiconductor Division introduced a commercial photovoltaic product with 26% efficiency for US\$ 25 per cell with 14 MW peak power. The energy cost was US\$ 1785 per kW.

In 1957, Hoffman Electronics introduced a solar cell with 8% efficiency. A year later, in 1958, the same company introduced a solar cell with 9% efficiency. The first radiation proof silicon solar cell was produced for the needs of space

technology the same year. In 1959, Hoffman Electronics introduced commercially available solar cells with 10% efficiency. A year after, they introduced yet another solar cell with 14% efficiency. The first sun-powered automobile was demonstrated in Chicago, Illinois on August 31st, 1955. During the year 1962, the first commercial telecommunications satellite Telstar, developed by Bell Laboratories, was launched. It was powered by a photovoltaic system having a peak power of 14 W.

In 1963, Sharp Corporation developed the first commercial photovoltaic module from silicon solar cells. The biggest photovoltaic system at the time, the 242 W module field was set up in Japan. A year later, in 1964, Americans applied a 470 W photovoltaic field in the Nimbus space project.

### **1970 - 1979 : Establishment of the biggest photovoltaic companies**

In 1970, Solar Power Corporation was established. Three years later, in 1973, Solarex Corporation was established. At the Delaware University a solar photovoltaic-thermal hybrid system, one of the first photovoltaic systems for domestic application, was developed. A silicon solar cell of US\$ 30 per W was produced. In 1974, the Japanese Sunshine project commenced. A year later, in 1975, Solec International and Solar Technology International were established.

### **1980 - 1989 : Large standalone systems installations**

Many important events in the field of photovoltaics appeared in 1980. ARCO Solar was the first to produce photovoltaic modules with peak power of over 1 MW per year. BP entered solar industry via purchase of Lucas Energy Systems. A seawater desalination system with 10.8 Kw peak power was built in Jeddah, Saudi Arabia the same year. Helios Technology, the oldest European solar cells producer, was established. The world production of photovoltaic modules exceeded 9.3 MW in 1982. Volkswagen began testing photovoltaic systems placed on vehicle roofs with 160 W peak power for vehicle start up.

In 1984, a 1 MW photovoltaic power plant began to operate in Sacramento, California. ARCO Solar introduced the first amorphous modules. In 1985, researchers of the University of New South Wales in Australia constructed a solar cell with more than 20% efficiency. BP built a power plant in Sydney and shortly after another one in Madrid. In 1986, ARCO Solar introduced the first commercial thin film photovoltaic module. BP got a thin film technology patent for a solar cells production in 1989.

### **1990 - 1999 : Large photovoltaic companies co-operation**

In 1990, Energy Conversion Devices Inc. (ECD) and Canon Inc. established a joint company United Solar Systems Corporation for solar cells production. Siemens bought ARCO Solar and established Siemens Solar Industries, which is nowadays one of the biggest photovoltaic companies in the world. Founded in 1977, Solar Energy Research Institute (SERI) renamed to National Renewable Energy Laboratory (NREL). A year later, in 1991, BP Solar Systems renamed to BP Solar International (BPSI), and became an independent unit within British Petroleum concern. In 1996, BP Solar purchased APS production premises in California, and announced a commercial CIS (copper indium diselenide) solar cells production.

### **2000 - : Renewable energy and the Stock exchange**

Some photovoltaic and renewable energy resources companies now have shares listed, predominantly in the German stock exchange. Capital mergers in Germany led to large photovoltaic corporation establishments. During 2000 and 2001 production of Japanese producers increased significantly. Sharp and Kyocera each produce modules with peak power equivalent to the annual consumption in Germany. Sanyo is close as well.

### **1.3.2 Dye-Sensitized Solar Cells<sup>2</sup>**

In 1710, Diesbach produced the first synthetic dye, Prussian blue.[9] A century later, in 1837, Daguerre made the first photographic images. Fox Talbot followed with the silver halide process in 1839. Although the art of formulating photographic emulsions only became a science with the theoretical analysis of the process by Gurney and Mott in 1938,[10] there was constant progress in the overall sensitivity of photographic emulsions, which had been particularly poor for the green to red spectral region. This can now be recognized as due to the semiconductor nature of the silver halides crystals used in photography, whose band gaps range from 2.7 to 3.2 eV. So the photoresponse is negligible for wavelengths longer than 460 nm. It was noted, for example, that the origin of the gelatin used as the support medium for the silver halide grains significantly modified the film sensitivity. In the 20th century, it was demonstrated that an organosulphur compound present in calf skin gelatin was responsible,[11] and which is now known to have its effect by inducing a nanostructure of silver

---

<sup>2</sup>Adapted from McEvoy, A. J.; Gratzel, M. *Sol. Energy Mater.* 1994, 32, 221 and Gratzel, M. *Prog. Photovolt. Res. Appl.* 2000, 8, 171.

sulphide on each grain. It can, therefore, be regarded as the first sensitization at a semiconductor heterojunction. It is an interesting convergence of photography and photoelectrochemistry, both of which rely on photo-induced charge separation at a liquid-solid interface. As seen before, the silver halides have band gaps of the order of 2.7-3.2 eV, and are therefore insensitive to much of the visible spectrum. The first panchromatic film, able to render the image of a scene realistically into black and white, followed on the work of Vogel in Berlin after 1873,[12] in which he associated dyes with the halide semiconductor grains. The first sensitization of a photoelectrode by Moser followed shortly thereafter, using a similar idea.[13] It was confirmed by Rigollot in 1893.[14]

However, the clear recognition of the parallelism between the two procedures, a realization that the same dyes in principle can function in both[15] and a verification that their operating mechanism is by injection of electrons from photo-excited dye molecules into the conduction band of the n-type semiconductor substrates[16] date from the 1960s. In subsequent years, the idea developed that the dye could function most efficiently if chemisorbed on the surface of semiconductor.[17-19] The concept emerged to use dispersed particles to provide a sufficient interface,[20] then photoelectrodes with high surface roughness were employed.[21,22] Titanium dioxide became the semiconductor of choice. This material has many advantages for sensitized photochemistry and photoelectrochemistry: it is a low cost, widely available, non-toxic and biocompatible material, and as such is even used in health care products, as well as domestic applications such as paint pigmentation. The standard dye at the time was tris(2,2'-bipyridyl-4,4'-carboxylate) ruthenium(II), the function of the carboxylate being the attachment by chemisorption of the chromophore to the oxide substrate. Progress thereafter, until the announcement in 1991 of the sensitized nanocrystalline photovoltaic device with a conversion efficiency at that time of 7.1% under solar illumination,[23] was incremental, a synergy of structure, substrate roughness and morphology, dye photophysics and electrolyte redox chemistry. That evolution has continued progressively since then, with a certified efficiency of now over 10%.

## 1.4 References of Chapter 1

- [1] Chow, J.; Kopp, R. J.; Portney, P. R. *science* 2003, 302, 1528.
- [2] Global atmospheric concentration of CO<sub>2</sub>, 1999.
- [3] Energy, E. C. F. [http://europa.eu.int/comm/energy/res/sectors/bioenergy\\_en.htm](http://europa.eu.int/comm/energy/res/sectors/bioenergy_en.htm).
- [4] Becquerel, A. E. C. R. Acad. Sci. Paris 1839, 9, 561.
- [5] Smith, W. *Nature* 1873, 303.
- [6] Adams, W. G.; Day, R. E. *Proc. R. Soc. Lond. A* 1877, 25, 113.
- [7] Einstein, A. *Ann. Phys.* 1905, 17, 132.
- [8] Czochralski, J. Z. *Phys. Chem.* 1918, 92, 219.
- [9] *Observ. Misc. Berolinens. ad incrementum scientiarum.* 1710, 377. Berlin.
- [10] Gurney, R. W.; Mott, N. F. *Proc. R. Soc. Lond. A* 1938, 164, 151.
- [11] James, T. H. *The Theory of the Photographic Process*, 4th. ed.; Macmillan: New York, 1977.
- [12] West, W. *Proceedings of the Vogel Centennial Symposium. Photogr. Sci. Eng.* 1974, 18,35.
- [13] Moser, J. *Monatsch. Chem.* 1887, 8, 373.
- [14] Rigollot, H. C. R. Acad. Sci. Paris 1893, 116, 561.
- [15] Namba, S.; Hishiki, Y. *J. Phys. Chem.* 1965, 69, 774.
- [16] Gerischer, H.; Tributsch, H. *Ber. Bunsenges. Phys. Chem.* 1968, 72, 437.
- [17] Dare-Edwards, M. P.; Goodenough, J. B.; Hammett, A.; Seddon, K. R.; Wright, R. D. *Faraday Disc. Chem. Soc.* 1980, 70, 285.
- [18] Tsubomura, H.; Matsumura, M.; Noyamaura, Y.; Amamiya, T. *Nature* 1976, 261, 402.
- [19] Clark, W. D. K.; Sutin, N. *J. Am. Chem. Soc.* 1984, 99, 676.
- [20] Duonghong, D.; Serpone, N.; Gratzel, M. *Helv. Chim. Acta* 1984, 67, 1012.
- [21] Desilvestro, J.; Gratzel, M.; Kavan, L.; Moser, J.; Augustynski, J. *J Am Chem Soc* 1985, 107, 2988.
- [22] Vlachopoulos, N.; Liska, P.; Augustynski, J.; Gratzel, M. *J. Am. Chem. Soc.* 1988, 101, 1216.
- [23] O'Regan, B.; Gratzel, M. *Nature* 1991, 353, 737

# Chapter 2

## Photovoltaic technologies<sup>1</sup>

### 2.1 Silicon

Silicon is the most popular solar-cell material for commercial applications because it is so readily abundant (it is actually the second most abundant element in the Earth's crust-second only to oxygen). However, to be useful in solar cells, it must be refined to 99.9999% purity. Therefore the process of purification is

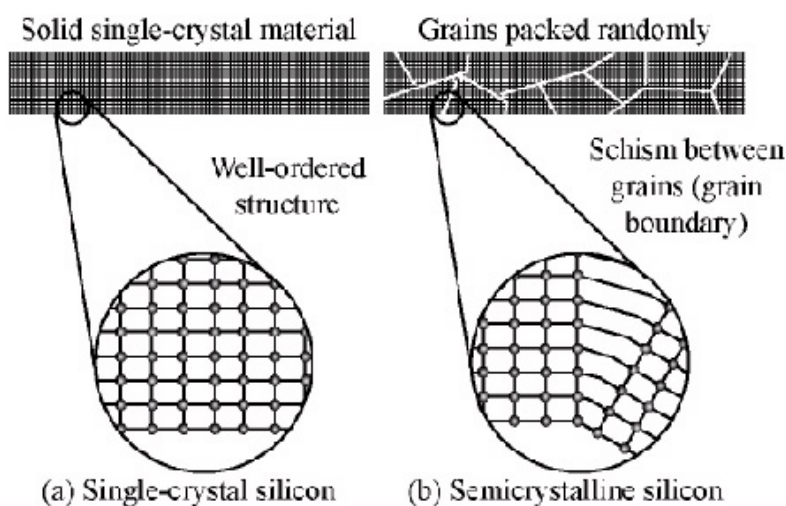


Figure 2.1: Single-crystal material (a) is structurally uniform; there are no disturbances in the orderly arrangement of atoms. Semicrystalline material (b) is made up of several crystals or "grains". At the interfaces of the grains, or "boundaries", the atomic order is disrupted. Here, electrons are more likely to recombine with holes rather than contribute to the electrical circuit

expensive. A photovoltaic cell is made of two layers of silicon, which are doped to polarize the junction. To make one of the layers positive, a certain number of atoms of p-type element, like boron, can be incorporated into it. To negatively charge the other layer, a certain number of n-type atoms, like phosphorus, can also be incorporated. When a photon having enough energy is absorbed in this semiconductor, it excites an electron from the valence band into the conduction

<sup>1</sup>Adapted from <http://www.eere.energy.gov/pv> ©NREL, U.S. Department of Energy.

band, leaving a positively charged hole. This is called the photovoltaic effect. This effect creates a potential difference across a junction of two different materials. Crystalline silicon (c-Si) is used in several forms: single-crystalline or monocrystalline silicon, multicrystalline or polycrystalline silicon, ribbon and sheet silicon and thin-layer silicon (Figure 2.1).

### 2.1.1 Si (single-crystal)

In single-crystal silicon, the molecular structure of the material is uniform because the entire structure is grown from the same or a single crystal. This uniformity is ideal for efficiently transferring electrons through the material. To make an effective photovoltaic cell, silicon is doped to make it n-type and p-type. Figure 2.1. Single-crystal material (a) is structurally uniform; there are no disturbances in the orderly arrangement of atoms. Semicrystalline material (b) is made up of several crystals or "grains".

At the interfaces of the grains, or "boundaries", the atomic order is disrupted. Here, electrons are more likely to recombine with holes rather than contribute to the electrical circuit.

To produce the single-crystal, we first melt the high-purity silicon. We then cause it to reform very slowly in contact with a single crystal seed. The silicon adapts to the pattern of the single crystal seed as it cools and solidifies gradually. Not surprisingly, because we start from a seed, this process is called growing a new ingot of single-crystal silicon out of the molten silicon. Several specific processes can be used to accomplish this. The most established and dependable means are the Czochralski method and the floating-zone (FZ) technique. In the Czochralski process, a seed crystal is dipped into a crucible of molten silicon and withdrawn slowly, pulling a cylindrical single crystal as the silicon crystallizes on the seed (Figure 2.2).

The float zone (FZ) process produces purer crystals, because they are not contaminated by the crucible as Czochralski crystals are. In the FZ process, a silicon rod is set atop a seed crystal and lowered through an electromagnetic coil. The coil's magnetic field induces an electric field in the rod, heating and melting the interface between the rod and the seed. Single-crystal silicon forms at the interface, growing upward as the coils are slowly raised.

Once the single-crystal ingots are produced, they must be sliced to form wafers.

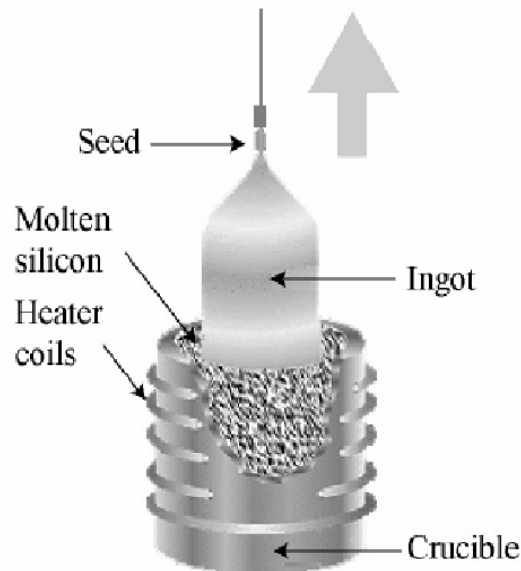


Figure 2.2: The most widely used technique for making single-crystal silicon is the Czochralski process, in which seed of single-crystal silicon contacts the top of molten silicon. As the seed is slowly raised, atoms of the molten silicon solidify in the pattern of the seed and extend the single-crystal structure. ©US Department of Energy, USA

Although single-crystal silicon technology is well developed, the Czochralski, FZ, and ingotcasting processes are complex and expensive. A group of new crystal-producing processes, however, generally called shaped-ribbon growth, could reduce processing costs by forming silicon directly into thin, usable wafers of single-crystal silicon. These methods involve forming thin crystalline sheets directly, thereby avoiding the slicing step required of cylindrical ingots. These crystals are then cut in ultra-fine layers, doped and connected. The monocrystalline cells allow high efficiencies, in the order of 15% to 25%.

These cells nevertheless suffer from two backdraws: their high price and their long pay off time of the energy investment. This pay off time is the time during which a solar cell must produce electricity in order to repay the energy that was necessary to produce it. This time can be as long as 7 years for monocrystalline cells. They are nevertheless appropriate for applications requiring high performances, such as electro-solar cars.

### 2.1.2 Si (multicrystalline)

Multicrystalline silicon consists of several smaller crystals or grains, which introduce boundaries. These boundaries impede the flow of electrons and encourage them to recombine with holes and thereby reduce the power output of the cell. However, multicrystalline silicon is much cheaper to produce than

single-crystalline silicon, so researchers are working on other ways of minimizing the effects of grain boundaries.

Multicrystalline silicon can be produced in a variety of ways. The most popular commercial methods involve a casting process in which molten silicon is directly cast into a mold and allowed to solidify into an ingot (Figure 2.3).

Generally, the mold is square, producing an ingot that can be cut and sliced into square cells to fit more compactly into a photovoltaic module.

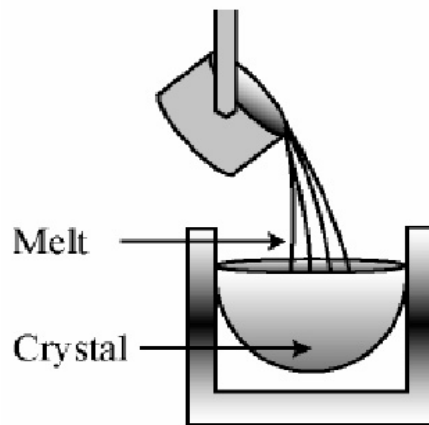


Figure 2.3: The most popular method for making commercial multicrystalline silicon is casting, in which molten silicon is poured directly into a mold and allowed to solidify into an ingot

### 2.1.3 Si (thin-film transfer)

Solar cells based on monocrystalline silicon wafers reached a conversion efficiency close to 25%, and it has been demonstrated that a wafer thinned down to about  $50\mu\text{m}$  still allows one to obtain a cell efficiency of 21.5%. [1]

Unfortunately, the thinning of wafers is not suitable for minimizing material expenses and therefore will not lead to decreased production costs. In order to enable economically viable thin film technologies several processes employing the transfer of monocrystalline silicon films onto alternative substrates are currently under investigation by research groups around the world.[2-6]

Monocrystalline silicon thin film solar processed by layer transfer using the quasi-monocrystalline silicon (QMS) approach have demonstrated high efficiencies (Figure 2.4). [7]

Chemical vapor deposition serves to epitaxially deposit silicon on QMS films obtained from thermal crystallization of a double layer porous silicon film on a

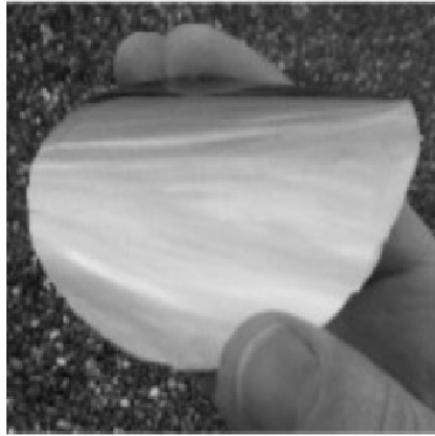


Figure 2.4: Photograph of a  $14\ \mu\text{m}$  thick epitaxial silicon film on top of a  $1.5\ \mu\text{m}$  thick QMS film, transferred to a plastic foil.

silicon wafer. A separation layer that forms during this crystallization process allows one to separate the epitaxial layer on top of the quasi-monocrystalline film from the starting silicon wafer after solar cell processing.

Independently confirmed thin film solar cell efficiencies are 15.4% and 16.6% for thin film solar cells transferred to a glass superstrate with a total silicon film thickness of  $24.5\ \mu\text{m}$  and  $46.5\ \mu\text{m}$ , respectively, and a cell area of  $4\ \text{cm}^2$ . Device simulations indicate an efficiency potential above 20% with material parameters accessible today by introducing an additional back surface reflector.

## 2.2 III-V cells

These photovoltaic technologies, based on Group III and V elements in the Periodic Table, show very high conversion efficiencies under either normal sunlight or sunlight that is concentrated (Figure 2.5). Single-crystal cells of this type are usually made of gallium arsenide (GaAs). Gallium arsenide can be alloyed with elements such as indium, phosphorus, and aluminum to create semiconductors that respond to different spectral energies.

Gallium is a by-product of the smelting of other metals, notably aluminum and zinc, and it is rarer than gold. Arsenic is not rare, but it is poisonous. Gallium arsenide's use in solar cells has been developing synergistically with its use in light-emitting diodes, lasers, and other optoelectronic devices.

GaAs is especially suitable for use in multijunction (see "Multijunction cells", page 31) and high-efficiency solar cells for several reasons:

1. The GaAs band gap is 1.43 eV, nearly ideal for single-junction solar cells.



Figure 2.5: To be cost-effective for terrestrial use, GaAs high-efficiency cells are more appropriate for concentrator systems such as this one at Sandia National Laboratories. ©Sandia National Laboratories, USA

2. GaAs has an absorptivity so high it requires a cell only a few microns thick to absorb sunlight (crystalline silicon requires a layer 100 microns or more in thickness).
3. Unlike silicon cells, GaAs cells are relatively insensitive to heat (cell temperatures can often be quite high, especially in concentrator applications).
4. Alloys made from GaAs using aluminum, phosphorus, antimony, or indium have characteristics complementary to those of gallium arsenide, allowing great flexibility in cell design.
5. GaAs is very resistant to radiation damage. This, along with its high efficiency, makes GaAs very desirable for space applications.

One of the greatest advantages of gallium arsenide and its alloys as photovoltaic cell materials is the wide range of design options possible. A cell with a GaAs base can have several layers of slightly different compositions that allow a cell designer to precisely control the generation and collection of electrons and holes (again, see "Multijunction cells", page 31).

The greatest barrier to the success of GaAs cells has been the high cost of a single-crystal GaAs substrate. For this reason, GaAs cells are used primarily in concentrator systems, where the typical concentrator cell is about  $0,25\text{cm}^2$  in area and can produce ample power under high concentrations. In this configuration, the cost is low enough to make GaAs cells competitive, assuming that module efficiencies can reach between 20% and 25% and that the cost of the rest of the system can be reduced.

## 2.3 Polycrystalline thin film

One of the scientific discoveries of the computer semiconductor industry that has shown great potential for the photovoltaic industry is thin-film technology. Thin film photovoltaic cells use layers of semiconductor materials only a few micrometers thick, attached to an inexpensive backing such as glass, flexible plastic, or stainless steel (Figure 2.6). Semiconductor materials for use in thin films include amorphous silicon (a-Si) (see "Silicon", page 19), copper indium diselenide (CIS), and cadmium telluride (CdTe). Because the quantity of semiconductor material required for thin films is far smaller than for traditional photovoltaic cells, the cost of thin film manufacturing is far less than for crystalline silicon solar cells.

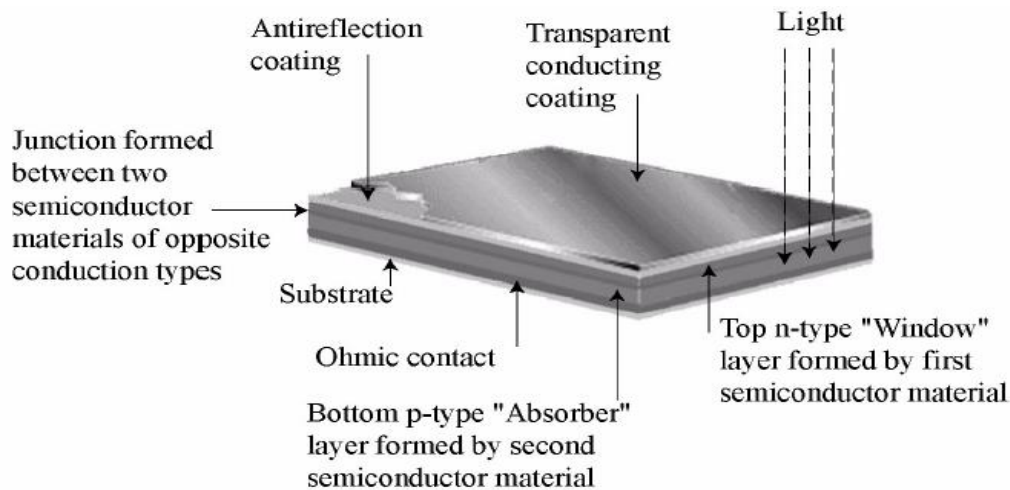


Figure 2.6: Polycrystalline thin-film cells have a heterojunction structure, in which the top layer is made of a different semiconductor material than the bottom semiconductor layer. The top layer, usually n-type, is a window that allows almost all of the light through to the absorbing layer, usually p-type. An ohmic contact is often used to provide a good electrical connection to the substrate

Rather than growing, slicing, and treating a crystalline ingot (required for single-crystal silicon), a thin layers of the required materials is sequentially deposited. Several different deposition techniques are available, and all of them are potentially cheaper than the ingot-growth techniques required for crystalline silicon. These deposition processes can be scaled up easily so that the same technique used to make a  $5\text{cm} \times 5\text{cm}$  laboratory cell can be used to make a  $60\text{cm} \times 150\text{cm}$  module.

Single-crystal cells have to be individually interconnected into a module, but thin-film devices can be made as a single unit. Layer upon layer is deposited sequentially on a glass superstrate, from the antireflection coating and conducting oxide, to the semiconductor material and the back electrical contacts.

Unlike most single-crystal cells, the typical thin-film device does not use a

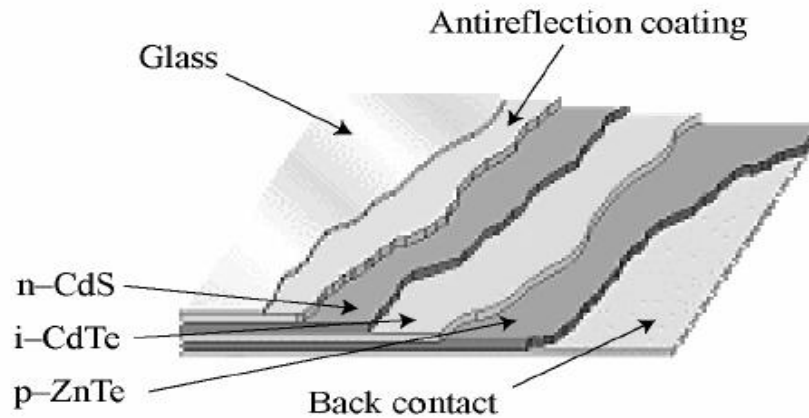


Figure 2.7: One way around contacting problems inherent in typical CdTe cells is to use an n-i-p structure, with an intrinsic layer of CdTe sandwiched between an n-type CdS layer and a p-type ZnTe layer

metal grid for the top electrical contact. Instead, it uses a thin layer of a transparent conducting oxide, such as tin oxide. These oxides are highly transparent and conduct electricity very well (see "TCO substrate", page 37). A separate antireflection coating may be used to top off the device, or the transparent conducting oxide may serve this function as well (Figure 2.7).

## 2.4 Amorphous silicon

Amorphous solids, like common glass, are materials in which the atoms are not arranged in any particular order. They do not form crystalline structures at all, and they contain large numbers of structural and bonding defects. They also come from the cuttings from crystal blocks, but these blocks are cast and therefore heterogeneous. Difficulties linked to big crystal growth are then avoided. Efficiency for amorphous silicon cells, in the order of 10%, is slightly lower, but is largely compensated by lower production costs. Producing such cells need less energy (Figure 2.8).

It wasn't until 1974 that researchers began to realize that amorphous silicon could be used in photovoltaic devices by properly controlling the conditions under which it was deposited and by carefully modifying its composition (Figure 2.9). Today, amorphous silicon is commonly used for solar-powered consumer devices that have low power requirements (e.g., wrist watches and calculators).

Amorphous silicon absorbs solar radiation 40 times more efficiently than does single-crystal silicon, so a film only about 1 micron thick can absorb 90% of the usable solar energy. This is one of the most important factors affecting its low cost potential. Other principal economic advantages are that amorphous

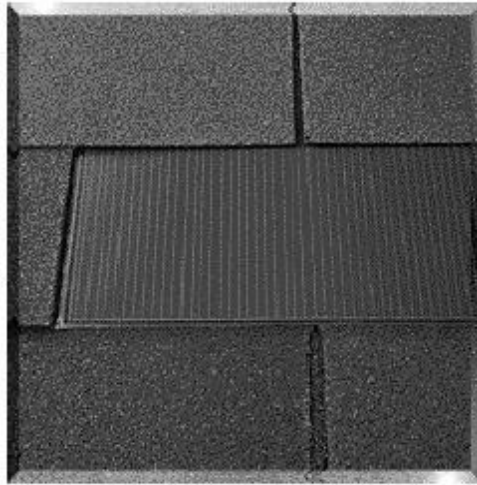


Figure 2.8: The versatility of amorphous silicon is shown in this flexible roof shingle module. The shingle can be built right into new homes where covenants would prohibit more conventional photovoltaic modules. ©NREL

silicon can be produced at a lower temperature and can be deposited on lowcost substrates. These characteristics make amorphous silicon the leading thin-film photovoltaic material.

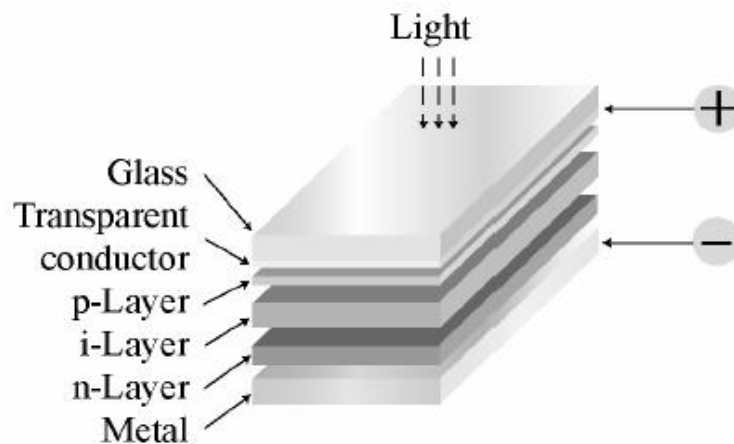


Figure 2.9: The typical amorphous silicon cell employs a p-i-n design, in which an intrinsic layer is sandwiched between a p layer and an n layer

Because amorphous silicon does not have the structural uniformity of crystalline or even multicrystalline silicon, the small deviations result in defects such as non-bonding electrons, where atoms are missing a neighbor to which they can bond. These defects provide places for electrons to recombine with holes rather than contributing to the electrical circuit. Ordinarily, such a material would be unacceptable for electronic devices because the defects limit the flow of current.

But if amorphous silicon is deposited in such a way that it contains a small amount of hydrogen (through a process called hydrogenation), then the hydrogen atoms combine chemically with many of the non-bonding electrons and

thereby permitting electrons to move through the amorphous silicon (Figure 2.10).

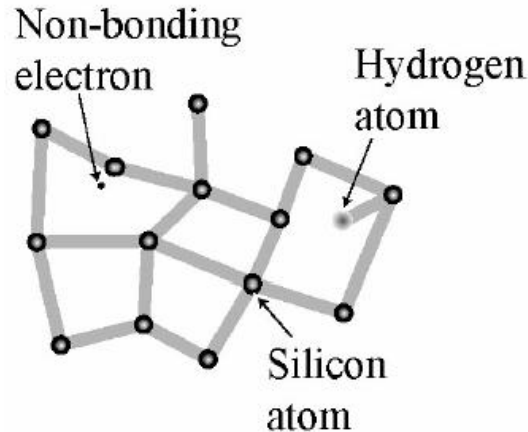


Figure 2.10: Amorphous silicon's random structural characteristics result in deviations like non-bonding electrons. This provides places for electrons to recombine with holes, but this may be neutralized somewhat with atomic hydrogen

## 2.5 Photoelectrochemical cells

### 2.5.1 Nanocrystalline Dye-Sensitized Solar Cells

In contrast to the conventional systems, where the semiconductor assumes both the task of light absorption and charge carrier transport, the two functions are separated in the Dye-Sensitized Solar Cells (DSSC).

Light is absorbed by a sensitizer which is anchored to the surface of a wide band gap semiconductor. Charge separation takes place in the dye via photo-induced electron injection from the dye into the conduction band of the solid. Carriers are transported in the conduction band of the semiconductor to the charge collector. The use of transition metal complexes having a broad absorption band in conjunction with oxide films of nanocrystalline morphology permits the harvesting of a large fraction of sunlight. Near-quantitative conversion of incident photons into electric current is achieved over a large spectral range extending over the whole visible region. Overall solar (standard AM1,5) to electric conversion efficiencies over 10% have been reached.

## 2.6 Multijunction cells

Most common photovoltaic devices use a single junction, or interface, to create an electric field within a semiconductor such as a photovoltaic cell. In a single-

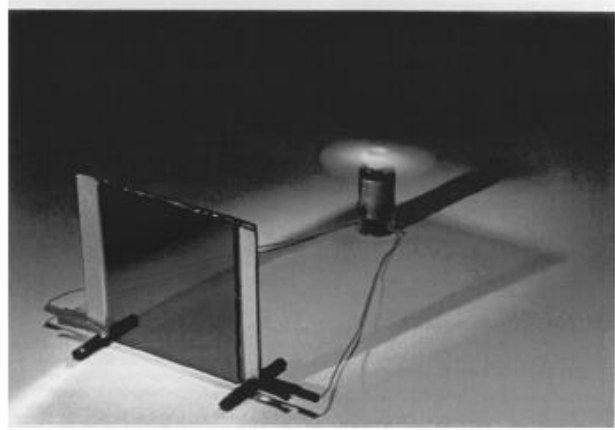


Figure 2.11: A transparent Dye-Sensitized Solar Cell running a small motor under a diffuse day-light. ©EPFL-LPI

junction photovoltaic cell, only photons whose energy is equal to or greater than the band gap of the cell material can free an electron for an electric circuit. In other words, the photovoltaic response of single-junction cells is limited to the portion of the sun's spectrum whose energy is above the band gap of the absorbing material, and lower-energy photons are not used.

One way to get around this limitation is to use two or more different cells, with more than one band gap and more than one junction, to generate a voltage. These are referred to as multijunction cells (also called cascade or tandem cells). Multijunction devices can achieve a higher total conversion efficiency because they can convert more of the energy spectrum of light to electricity (Figure 2.12). In a typical multijunction photovoltaic cell, individual single-junction

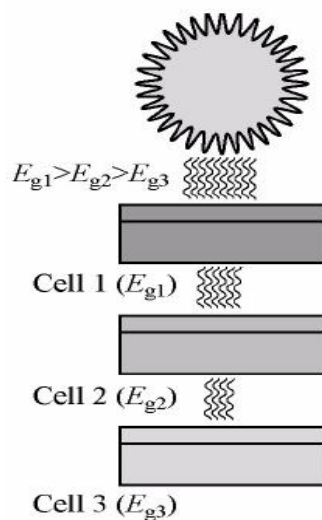


Figure 2.12: A multijunction device is a stack of individual single-junction cells in descending order of band gap ( $E_g$ ). The top cell captures the high-energy photons and passes the rest of the photons on to be absorbed by lower-band-gap cells

cells with different energy band gaps are stacked on top of one another. Sunlight then falls first on the material with the largest band gap, and the highest-energy photons are absorbed. Photons not absorbed in the first cell continue on to the second cell, which absorbs the higher-energy portion of the remaining solar radiation while remaining transparent to the lower-energy photons. Much of the work in this area uses gallium arsenide and its alloys, as well as using amorphous silicon, copper indium diselenide, and gallium indium phosphide (Figure 2.13). Although two-junction cells have been built, most research is

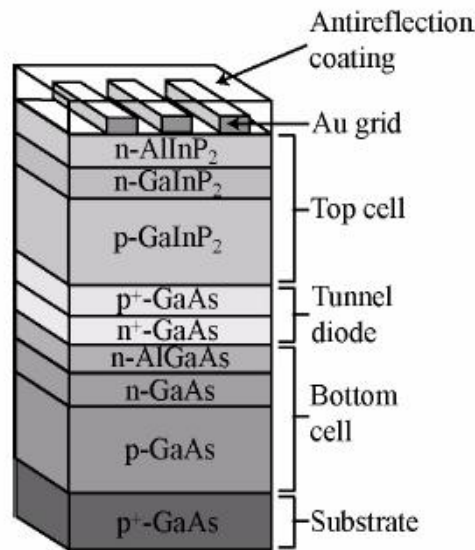


Figure 2.13: This multijunction device uses a top cell of gallium indium phosphide, a tunnel junction, to aid the flow of electrons between the cells, and a bottom cell of gallium arsenide

focusing on three-junction and four-junction devices, using materials such as germanium (Ge) to capture the lowest-energy light in the lowest layer.

## 2.7 References of Chapter 2

- [1] Wang, A.; Zhao, J.; Wenham, S. R.; Green, M. A. Prog. Photovolt.: Res. & Appl. 1996, 4, 55.
- [2] Brendel, R.; Scholten, D. Appl. Phys. A 1999, 69, 201.
- [3] Brendel, R.; Auer, R.; Artmann, H. Prog. Photovolt.: Res. & Appl. 2001, 9, 217.
- [4] Nishida, S.; Nakagawa, K.; Iwane, M.; Iwasaki, Y.; Ukiyo, N.; Mizutani, M.; Shoji, T. Sol. Energy Mater. 2001, 65, 525.
- [5] Tayanaka, H.; Yamauchi, K.; Matsushita, T. Thin-film Crystalline Silicon Solar Cells Obtained by Separation of a Porous Silicon Sacrificial Layer; Proc. 2nd World Conf. on Photovolt. Solar Energy Conversion. 1998, 1272. Ispra.
- [6] Weber, K. J.; Catchpole, K.; Blakers, A. W. Crystal Growth 1998, 186, 369.
- [7] Rinke, T. J.; Bergmann, R. B.; Werner, J. H. Appl. Phys. A 1999, 68, 705.

# Chapter 3

## Dye-Sensitized Solar Cell

### 3.1 Advantageous of the Dye-Sensitized Solar Cell

One major advantage of new generation DSSC in comparison to the conventional silicon based photovoltaic devices is low cost,  $0,48 - 0,64 S/Wp$  for a 10% efficient cell in comparison to  $(0.48 \times 6 - 0.64 \times 6) S/Wp$  for single crystal silicon cells [1]. Moreover it is claimed that these cells offer high overall photon-to-electric energy conversion efficiency [2] and long term stability [3] during solar cell operation conditions.

### 3.2 Dye-Sensitized Solar Cell components

The Dye-Sensitized Solar Cell technology developed at the Ecole Polytechnique Federal de Lausanne (EPFL) contains broadly five components: (i) a conductive mechanical support, (ii) a semiconductor film, (iii) a sensitizer, (iv) an electrolyte containing the  $I^-/I_3^-$  redox couple, and (v) a counter electrode with a platinum catalyst. The total efficiency of the cell depends on optimization and compatibility of each of these components.[4] Across-section of the Dye-Sensitized Solar Cell is shown in Figure (3.1). To a large extent, the nanocrystalline semiconductor film technology and the dye spectral response are mainly responsible for the high efficiency. The high surface area and the thickness of the semiconductor film yields a high optical density for the adsorbed dye, resulting in efficient light harvesting.[5] The sensitizers display a crucial role in harvesting of sunlight. To trap solar radiation efficiently in the visible and the near IR region of the solar spectrum requires engineering of sensitizers at a molecular level.[6] The electrochemical and photophysical properties of the ground and the excited states of the sensitizer have a significant influence on the charge transfer (CT) dynamics at the semiconductor interface. The open-circuit potential of the cell depends on the redox couple, which shuttles between the sensitizer and the counter electrode.[7]

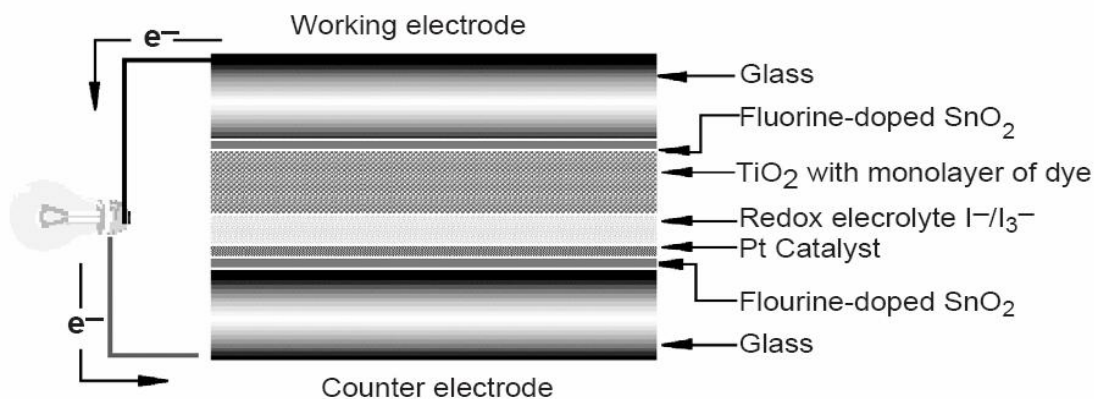


Figure 3.1: Schematic representation of the cross-section of a Dye-Sensitized Solar Cell

### 3.3 Dye-Sensitized Solar Cell Fabrication

Briefly, we describe here various steps involved in the preparation of Dye-Sensitized Solar Cell. The nanocrystalline  $TiO_2$  films were prepared by depositing  $TiO_2$  colloids on a transparent fluorine-doped tin oxide-conducting glass using either screen printing or by the doctor blade technique.[8,9] The films are then dried in air and fired at  $450^\circ\text{C}$ . The hot electrodes ( $\approx 80^\circ\text{C}$ ) are immersed into the dye solution, which is usually prepared in ethanol ( $2-5 \times 10^{-4}\text{M}$ ). The deposited dye film is used as a working electrode. A sandwich cell is prepared with a second piece of conducting glass coated with chemically deposited platinum from  $0.05\text{M}$  hexachloroplatinic acid. This platinum-coated counter electrode and the dye-coated  $TiO_2$  film are then put together with a thin transparent film of Surlyn polymer frame (DuPont). The sandwiched electrodes are tightly held and then heat is applied ( $130^\circ\text{C}$ ) around the Surlyn frame to seal the two electrodes. A thin layer of electrolyte containing the  $I_3^-/I^-$  redox couple in methoxyacetonitrile is introduced into the interelectrode space from the counter electrode side through predrilled holes. The drilled holes are sealed with a microscope cover slide and Surlyn to avoid leakage of the electrolyte solution. [7]

A module of a solar cell based on a dye-sensitized  $TiO_2$  nanocrystalline film is shown in Figure (3.2).

Small-area (less than  $1\text{cm}^2$ ) DSSC have achieved 10.8% efficiency by the EPFL group, and 8.23% in the ECN (Energy Research Centre for Netherlands) group for several square centimeters, but the efficiency of DSSC modules larger than  $100\text{cm}^2$  is still less than 7%. Recently, some European group obtained high efficiency in masterplate, but less than 30% active area in the DSSC [10]. The noneffective area will increase the cost of DSSC, and hide the merits of DSSC compared to Si-solar cell and other thin-film solar cells. Increasing the

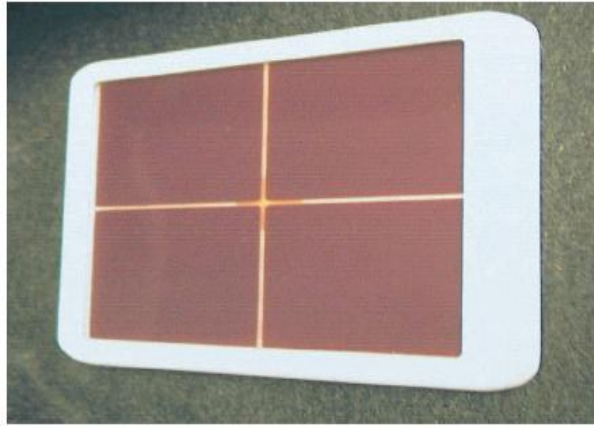


Figure 3.2: A module of a photoelectrochemical solar cell based on a dye-sensitized  $TiO_2$  nanocrystalline film

active area is one of the obstacles the DSSC have to overcome before it can be made into a commercial product.[11]

### 3.4 Operating Principles of the Dye-Sensitized Solar Cell

At the heart of the system is a wide band gap oxide semiconductor which is placed in contact with a redox electrolyte or an organic hole conductor. The material of choice has been  $TiO_2$  (anatase) although alternative wide band gap oxides such as ZnO [12], and  $Nb_2O_5$  [13] have also been investigated. Attached to the surface of the nanocrystalline film is a monolayer of the charge transfer dye. Photo-excitation of the latter results in the injection of an electron into the conduction band of the oxide. The original state of the dye is subsequently restored by electron donation from the electrolyte, usually an organic solvent containing redox system, such as the iodide/triiodide couple.

The regeneration of the sensitizer by iodide intercepts the recapture of the conduction band electron by the oxidized dye. The iodide is regenerated in turn by the reduction of triiodide at the counter-electrode the circuit being completed via electron migration through the external load. The voltage generated under illumination corresponds to the difference between the Fermi level of the electron in the solid and the redox potential of the electrolyte. Overall the device generates electric power from light without suffering any permanent chemical transformation.[14]

The details of the operating principles of the Dye-Sensitized Solar Cell are given in Figure (3.3).[7]

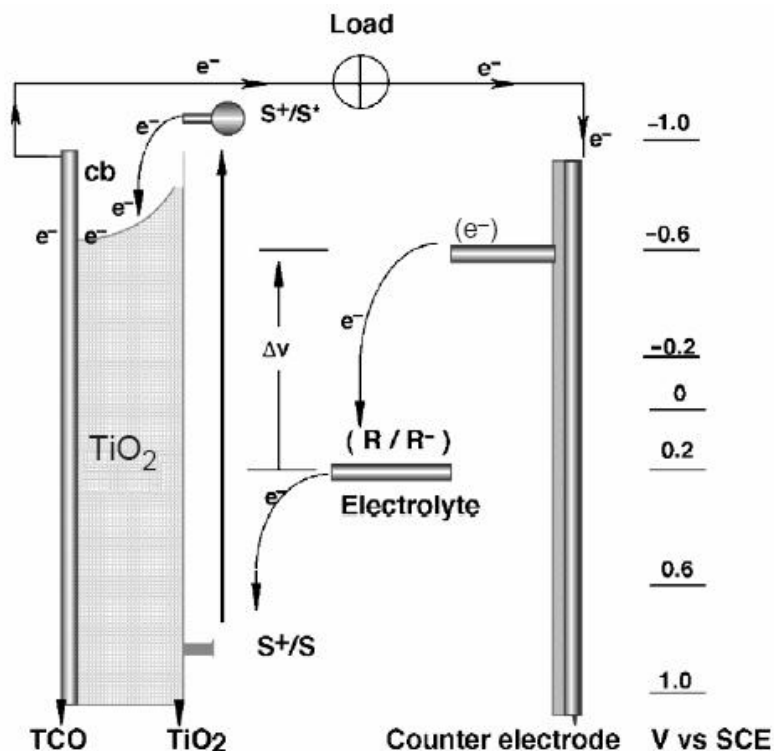
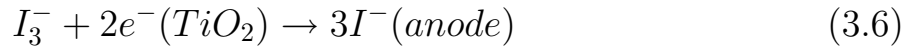
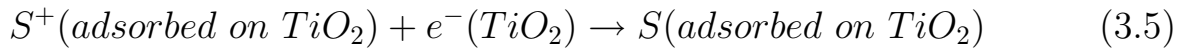
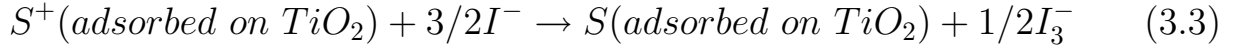
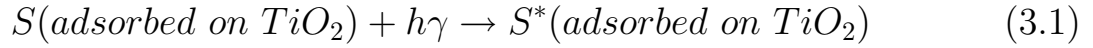


Figure 3.3: Operating principles and energy level diagram of a Dye-Sensitized Solar Cell.  $S/S^+/S^*$  = Sensitizer in the ground, oxidized and excited state, respectively.  $R/R^-$  = redox mediator ( $I_3^-/I^-$ ).[4]

### 3.5 Electron transfer dynamics [7]

Photoexcitation of the metal-to-ligand charge transfer (MLCT) of the adsorbed sensitizer (Equation (4.1)) leads to injection of electrons into the conduction band of the oxide (Equation (4.2)). The oxidized dye is subsequently reduced by electron donation from an electrolyte containing the iodide/triiodide redox system (Equation (4.3)). The injected electron flows through the semiconductor network to arrive at the back contact and then through the external load to the counter electrode. At the counter electrode, reduction of triiodide in turn regenerates iodide (Equation (4.4)) through the donation of electrons from the external circuit, which completes the circuit. With a closed external circuit and under illumination, the device then constitutes a photovoltaic energy conversion system, which is regenerative and stable. However, there are undesirable side reactions: the injected electrons may recombine either with oxidized sensitizer (Equation (4.5)), or with the oxidized redox couple at the  $TiO_2$  surface (Equation (4.6)), resulting in losses in the cell efficiency. For a net forward current under steady state illumination, the processes of Equations (4.2) and (4.3) must be kinetically more favorable than Equations (4.5) and (4.6):



### 3.6 Semiconductor Films

The favored semiconductor materials titanium dioxide because of its abundance, low cost and nontoxicity. This last characteristic promotes its use in healthcare products and paints. the efficiency of the solar cell depends to a large extent on the nanocrystalline semiconductor films; the high surface area of these films yields a high dye loading and, therefore, high optical density, resulting in efficient light absorption. The nanoporous structure permits surface coverage of the dye to be sufficiently high for total absorption of the incident light, necessary for efficient solar energy conversion, since the area available for monomolecular distribution of adsorbate is 2-3 orders of magnitude higher than the geometric area of the substrate. [7]

### 3.7 Importance of morphology of $TiO_2$ films

The properties of  $TiO_2$  film have a significant influence on the photoelectrochemical performance of the DSSC.

The roughness factor (rf) of  $TiO_2$  film decreased as the particle size of  $TiO_2$  crystallites increased . The average pore size and porosity of the film decreased

with decreasing particle size because the void between the particles became smaller with the decrease of the particle size. [15]

So we can act the porosity of the  $TiO_2$  film by controlling the particle size and the average pore size.

The thickness of the  $TiO_2$  film is very important for the transportation of electrons as well as adsorption of the dye.

A relationship between nanocrystalline- $TiO_2$  film thickness and the resultant DSSC conversion efficiency was shown in Figure (3.4). The optimum film thickness to produce highly efficient DSSC being 12-14  $\mu m$ . [16,17].

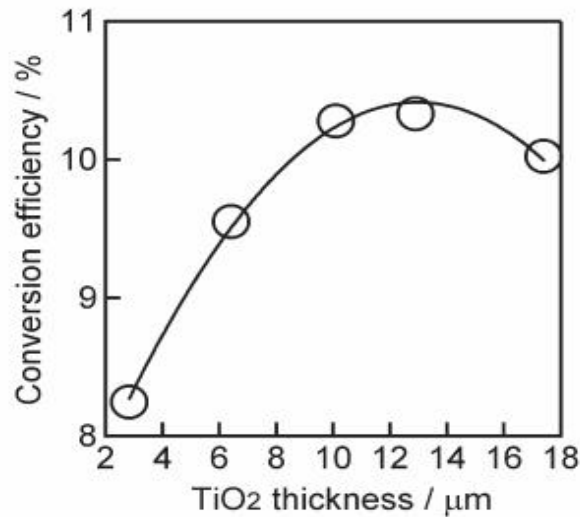


Figure 3.4: Photoconversion efficiency as a function of nanocrystalline  $TiO_2$  layer thickness. Illuminated- $TiO_2$  and aperture areas of cells are  $0.16 cm^2$  and  $0.25 cm^2$ , respectively [17]

### 3.8 Requirements of the Sensitizers [7]

The optimal sensitizer for the Dye-Sensitized Solar Cell should be panchromatic, i.e., it should absorb visible light of all colors. Ideally, all photons at wavelengths shorter than a threshold of about  $920nm$  should be harvested and converted to electric current.[18,19 ]In addition, the sensitizer should fulfill several other demanding conditions:

1. It must be firmly grafted onto the semiconductor oxide surface, and inject electrons into the conduction band with a quantum yield of unity.
2. (ii) The excited state of the dye must be higher in energy than the conduction band edge of the semiconductor, in order to inject electrons quantitatively.

3. The ground state redox potential of the dye should be sufficiently high that it can be regenerated rapidly via electron donation from the electrolyte or a hole conductor.
4. The extinction coefficient of the dye should be high over the whole absorption spectrum to absorb most of the incident light.
5. The dye should be soluble in some solvent for adsorption on  $TiO_2$  surface, and should not be desorbed by the electrolyte solution.
6. It should be stable enough to sustain at least 108 redox turnovers under illumination, corresponding to about 20 years of exposure to natural-sun light. Molecular engineering of ruthenium complexes that can act as panchromatic CT sensitizers for  $TiO_2$ -based solar cells presents a challenging task as several requirements have to be fulfilled by the dye, which are very difficult to be met simultaneously. The lowest unoccupied molecular orbitals (LUMOs) and the highest occupied molecular orbitals (HOMOs) have to be maintained at levels where photo-induced electron transfer into the  $TiO_2$  conduction band and regeneration of the dye by iodide can take place with practically 100% yield.

### 3.9 The general structure of the dye

Metal complex sensitizers usually have anchoring (carboxylated) ligands (Fig 3.5) for adsorption onto the semiconductor surface [20]. The dyes having the general structure of  $ML_2(X)_2$ , where L stands for 2,20 bipyridyl-4-40-dicarboxylic acid, M for ruthenium or osmium and X for halide, cyanide, thiocyanate, or water have been found promising [21-23]. The excitation of Ru complexes via photon absorption is of metal to ligand charge transfer (MLCT) type. This means that the highest occupied molecular orbital (HOMO) of the dye is localized near the metal atom, Ru in this case, whereas the lowest unoccupied molecular orbital (LUMO) is localized at the ligand species, in this case at the bipyridyl rings. At the excitation, an electron is lifted from the HOMO level to the LUMO level. Furthermore, the LUMO level, extending even to the COOH anchoring groups [21], is spatially close to the  $TiO_2$  surface, which means that there is significant overlap between electron wavefunctions of the LUMO level of the dye and the conduction band of  $TiO_2$ . This directionality of the excitation is proposed as one of the reasons for the fast electron transfer process at the dye- $TiO_2$  interface [21].

Cells based on this concept show energy conversion efficiencies up to 11% on small-area cells [24].

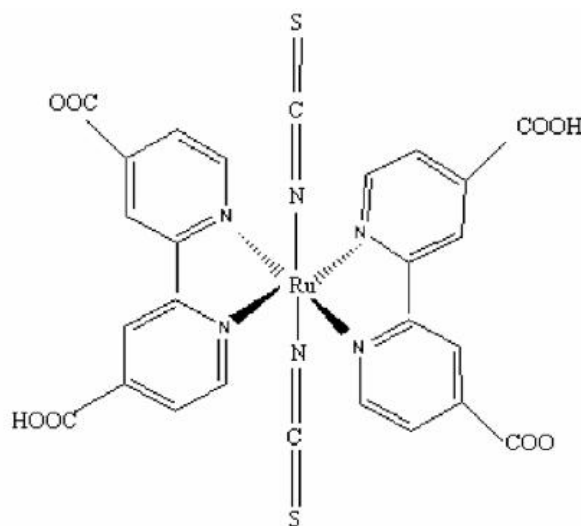


Figure 3.5: Chemical structure of a ruthenium dye

(Fig4.6) compares the spectral response of the photocurrent observed with the two sensitizers. The incident photon to current conversion efficiency (IPCE) of the DSSC is plotted as a function of excitation wavelength. Both chromophores show very high IPCE values in the visible range. However, the response of the black dye extends 100 nm further into the IR than that of N3. The photocurrent onset is close to 920 nm, i.e. near the optimal threshold for single junction converters.

From there on the IPCE rises gradually until at 700 nm it reaches a plateau of ca. 80%. If one accounts for reflection and absorption losses in the conducting glass the conversion of incident photons to electric currents is practically quantitative over the whole visible domain. [25,26]

An advantage of the DSSC with respect to competing technologies is that its performance is remarkably insensitive to temperature change. Thus, raising the temperature from 20 to 60° C has practically no effect on the power conversion efficiency. In contrast, conventional silicon cells exhibit a significant decline over the same temperature range amounting to ca. 20%. Since the temperature of a solar cell will reach readily 60° C under full sunlight this feature of the injection cell is particularly attractive for power generation under natural conditions. [25]

Another strategy to obtain a broad optical absorption extending throughout the visible and near IR region is to use a combination of two dyes which complement each other in their spectral features.

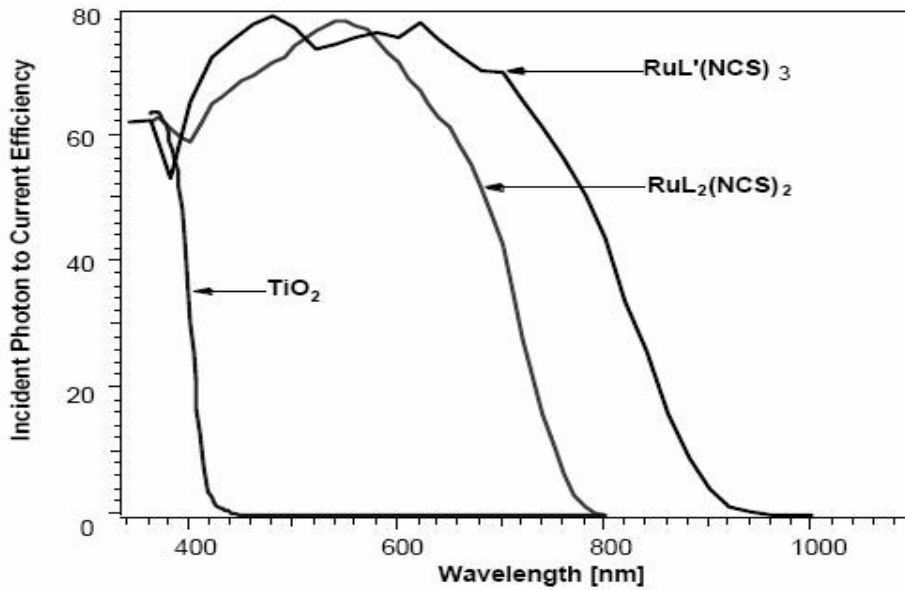


Figure 3.6: Photocurrent action spectra obtained with the  $N_3$  (ligand L) and the black dye (ligand L') as sensitizer. The photocurrent response of a bare  $TiO_2$  films is also shown for comparison

### 3.10 Electrolyte

Room temperature ionic liquid electrolytes have been actively pursued as non-volatile electrolytes of DSSC [27,28]. Molten salts based on imidazolium iodides have revealed very attractive stability features

### 3.11 Solid state Dye-Sensitized Solar Cells

In a solid state Dye-Sensitized Solar Cell the electrolyte is replaced with a p-type semiconductor or organic hole conductor materials [32-33] avoiding problems such as leakage of liquid electrolytes [34].

A solid state Dye-Sensitized Solar Cell is schematically shown in (Fig 3.7). The mesoporous metal oxide electrode, commonly,  $TiO_2$  is placed in contact with a solid state hole conductor. Attached to the surface of the nanocrystalline electrode film is a monolayer of the sensitizing dye. After the excitation of the dye an electron is injected into the conduction band of the semiconductor oxide electrode. The sensitizer dye is regenerated by the electron donation from the hole conductor [35].

In the solid state cell, the charge transport is electronic whereas when using liquid or polymer electrolyte, ionic transportation takes place [36].

The hole conductor must be able to transfer holes from the sensitizing dye

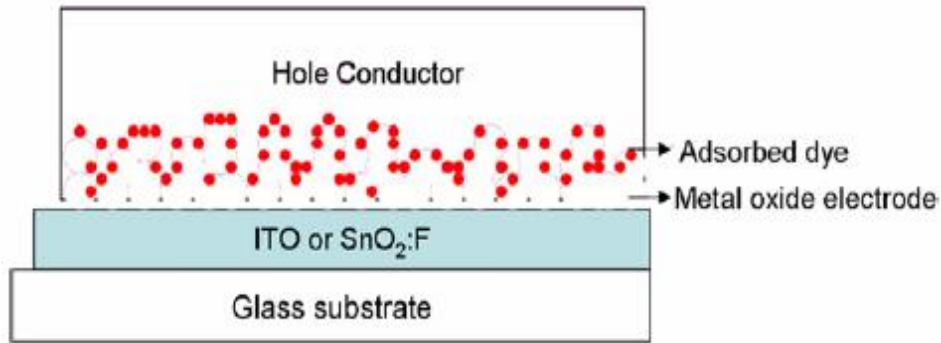


Figure 3.7: Schematic description of a solid state Dye-Sensitized Solar Cell

after the dye has injected electrons into the  $TiO_2$ ; that is, the upper edge of the valence band of ptype semiconductors must be located above the ground state level of the dye .(Fig 3.8)

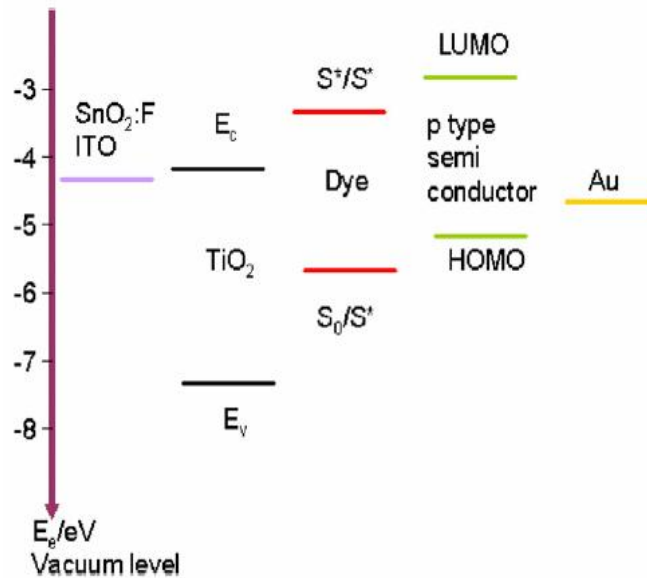


Figure 3.8: Energy diagram for an efficient charge transfer between solid state Dye-Sensitized Solar Cell components

Furthermore, hole conductors have to be deposited within the porous nanocrystalline layer penetrating into the pores of the nanoparticle and finally it must be transparent in the visible spectrum, or, if it absorbs light, it must be as efficient in electron injection as the dye. CuI, CuBr or CuSCN were found to be the successful candidates to replace the liquid electrolyte [37-40].

### 3.12 Counter electrodes

The counter electrode is one of the most important components in the Dye-Sensitized Solar Cell (DSSC). The task of the counter electrode (CE) is the reduction of the redox species used as a mediator in regenerating the sensitizer after electron injection, or collection of the holes from the hole conducting material in a solid-state DSSC [41]. At present, several different kinds of CEs have been introduced, for example: platinized transparent CEs, carbon CEs, and conductive polymer CEs [42,43].

The counter electrode is chosen according to the particular application of the DSSC. For power-producing windows or metal-foil-supported DSSC, one must employ a transparent counter electrode, e.g. a small amount of platinum deposited on F-doped tin oxide coated glass (FTO-glass) or plastic. [44] On the other hand, to make an inexpensive cell one should consider a low cost material such as a carbon catalyst for the CE [18]. Or, for "champion cells", one must choose the material for the CE with the lowest possible sheet resistance and a high rate of reduction of the redox electrolyte.

There are many different kinds of CEs. They can be divided into various groups: CEs prepared with a heating process, without a heating process, and with Pt and without Pt. The CEs prepared with a heating process show better results than without heating, however, these processes are impossible to apply to plastic substrates and non-heating processes are suitable for this application [41].

Platinum is an efficient catalyst but it can be replaced by other materials to obtain similar performances. Transparent CEs can be realized with a platinum catalyst on conducting glass. A combination of a low sheet resistance material such as SWCNT and a highly catalytically active material such as carbon black is promising for large DSSC modules [45].

### 3.13 References of Chapter 3

- [1] Smestad, G.;Bignozzi, C.; Argazzi, A., Sol. Energy Mater. Sol. Cells, 1994, 32, 256.
- [2] Nazeeruddin, M. K.; Kay, A.; Rodicio, I.; Humphry-Baker, R.; Muller, E.; Liska, P.; Vlachopoulos, N.; Gratzel, M. J. Am. Chem. Soc. 1993, 115, 6382.
- [3] Kohle, O.; Gratzel, M.; Meyer, A. F.; Meyer, T. B.; Adv. Mater. 1997, 9, 904.
- [4] Hagfeldt, A.; Gratzel, M. Chem. Rev. 1995, 95, 49-68.
- [5] Rothenberger, G.; Comte, P.; Gratzel, M. Sol. Energ. Mat. Sol. C. 1999, 58, 321-326.
- [6] Nazeeruddin, M. K.; Graetzel, M. Dyes for Semiconductor Sensitization. In Encyclopedia of Electrochemistry : Semiconductor Electrodes and Photoelectrochemistry, Vol. 6: Licht, S., Ed.; Wiley-VCH: 2002; Darmstadt, pp 407-431.
- [7] 2003 MD. K. Nazeeruddin and M. Graetzel. Published by Elsevier Ltd. Conversion and Storage of Solar Energy using Dye-sensitized Nanocrystalline TiO<sub>2</sub> Cells.
- [8]. Barbe, C. J.; Arendse, V.; Comte, P.; Jirousek, M.; Lenzmann, F.; Shklover, V.; Gratzel, M. J. Am. Ceram. Soc. 1997, 80, 3157-3171.
- [9]. Burnside, S. D.; Shklover, V.; Barbe, C. J.; Comte, P.; Arendse, F.; Brooks, K.; Gratzel, M. Chem. Mater. 1998, 10, 2419-2425. [10] M. Sp.ath, P.M. Sommeling, J.A.M. van Roosmalen, H.J.P. Smit, N.P.G. van der Burg, D.R. Mahieu, N.J. Bakker, J.M. Kroon, Photovolt.: Res. Appl. 11 (2003) 207-220.
- [11] Songyuan Dai\*, Jian Weng, Yifeng Sui, Chengwu Shi, Yang Huang, Shuanhong Chen, Xu Pan, Xiaqin Fang, Linhua Hu, Fantai Kong, Kongjia Wang. Solar Energy Materials & Solar Cells 84(2004) 125-133
- [12] K. Tennakone, G.R.R. Kumara, I.R.M. Kottegoda, V.S.P. Perera, Chem. Commun. (1999) 15.
- [13] K. Sayama, H. Suguhara, H. Arakawa, Chem. Mater. 10 (1998) 3825.
- [14] Michael Gratzel.; Journal of Photochemistry and Photobiology A: Chemistry 164 (2004) 3-14.
- [15] Songyuan Dai\*, Jian Weng, Yifeng Sui, Chengwu Shi, Yang Huang, Shuanhong Chen, Xu Pan, Xiaqin Fang, Linhua Hu, Fantai Kong, Kongjia Wang. Solar Energy Materials & Solar Cells 84 (2004) 125-133
- [16] Seigo Ito \*, Takurou N. Murakami 1, Pascal Comte 1,

- Paul Liska 1, Carole Gratzel 1, Mohammad K. Nazeeruddin 1, Michael Gratzel \*. *Thin Solid Films* (2007)
- [17] S. Ito, Md. K. Nazeeruddin, P. Liska, P. Comte, R. Charvet, P. Pechy, M. Jirousek, A. Kay, S.M. Zakeeruddin, M. Gratzel, *Prog. Photovolt.* 14 (2006) 589.
- [18]. Haught, A. F. J. *Sol. Ener. Engin.* 1984, 106, 3.
- [19]. De Vos, A. *Endoreversible Thermodynamics of Solar Energy Conversion*, Chapter 6, Oxford Science Publishers, Oxford, 1992.
- [20] A.S. Polo, M.K. Itokazu, N.Y.M. Iha, *Coord. Chem. Rev.* 248 (2004) 1343.
- [21] H. Halme, PhD thesis, Espoo (Finland), 2002.
- [22] A. Hagfeldt, M. Gratzel, *Acc. Chem. Res.* 33 (5) (2000) 269.
- [23] G. Sauve, M.E. Cass, G. Coia, S.J. Doig, I. Lauermann, K.E. Pomykal, N.S. Lewis, *J. Phys. Chem. B* 104 (2000) 6821.
- [24] B. O'Reagan, M. Graetzel, *Nature* 353 (1991) 737.
- [25] Michael Gratzel. *Journal of Photochemistry and Photobiology C: Photochemistry Reviews* 4 (2003) 145-153
- [26] Michael Gratzel *Journal of Photochemistry and Photobiology A: Chemistry* 164 (2004) 3-14
- [27] N. Papageorgiou, Y. Athanassov, M. Armand, P. Bonhote, H. Pettersson, A. Azam, M. Gratzel, *J. Electrochem. Soc.* 143 (1996) 3099.
- [28] S. Murai, S. Mikoshiba, H. Sumino, T. Kato, S. Hayase, *Chem. Commun.* (2003) 1534.
- [29] H. Matsumoto, T. Matsuda, T. Tsuda, R. Hagiwara, Y. Ito, Y. Miyazaki, *Chem. Lett.* (2001) 26.
- [30] P. Wang, S.M. Zakeeruddin, I. Exnar, M. Gratzel, *Chem. Commun.* (2002) 2972-2973.
- [31] P. Wang, S.M. Zakeeruddin, P. Comte, I. Exnar, M. Gratzel, *J. Am. Chem. Soc.* 125 (2003) 1166-1167.
- [32] K. Tennakone, G.R.R. Kumara, I.R.M. Kottegoda, K.G. U Wijayantha, V.P.S. Perrera, *J. Phys. D: Appl. Phys.* 31 (1998) 1492.
- [33] U. Bach, D. Lupo, P. Comte, J.E. Moser, F. Weissortel, J. Salbeck, H. Spreitzer, M. Gratzel, *Nature* 395 (1995) 583.
- [34] A. Fujishima, X.T. Zhang, *Proc. Jpn. Acad. B* 2 (2005) 33.
- [35] B. Li, L. Wang, B. Kang, P. Wang, Y. Qiu, *Sol. Energ. Mat. Sol. Cells* 90 (2006) 549.
- [36] A.F. Nogueira, C. Longo, M.A. De Paoli, *Coord.*

- Chem. Rev. 248  
(2004) 1455.
- [37] B. Oregan, D.T. Schwartz, Chem. Mater. 10 (1998) 1501.
- [38] K. Tennakone, G.R.R. A Kumara, A.R. Kumarasinghe,  
K.G.U. Wijayantha, P.M. Sirimanne, Semicond. Sci. Tech. 10  
(1995) 1689. [39] G.R.R.A. Kumara, A. Konno, G.K.R. Senadeera,  
P.V.V. Jayaweera, Dbra De Silva, K. Tennakone, Sol.  
Energ. Mat. Sol. Cells 69 (2001) 195.
- [40] K. Tennakone, G.K.R. Senadeera, Dbra De Silva, I.R.M.  
Kottegoda, Appl. Phys. Lett. 77 (2000) 2367.
- [41] Takurou N. Murakami a, Michael Graetzel , Inorganica Chimica  
Acta 361 (2008) 572-580.
- [42] Y. Saito, T. Kitamura, Y. Wada, S. Yanagida,  
Chem. Lett. 31 (2002) 1060.
- [43] Y. Saito, W. Kubo, T. Kitamura, Y. Wada,  
S. Yanagida, J. Photochem. Photobiol. A. Chem. 164 (2004) 153.
- [44] N. Papageorgiou, W.F. Maier, M. Gratzel,  
J. Electrochem. Soc. 144 (1997) 876.
- [45] K. Suzuki, M. Yamamoto, M. Kumagai, S. Yanagida,  
Chem. Lett. 32 (2003) 28.

# Chapter 4

## General properties of titanium dioxide

### 4.1 $TiO_2$ crystal structures

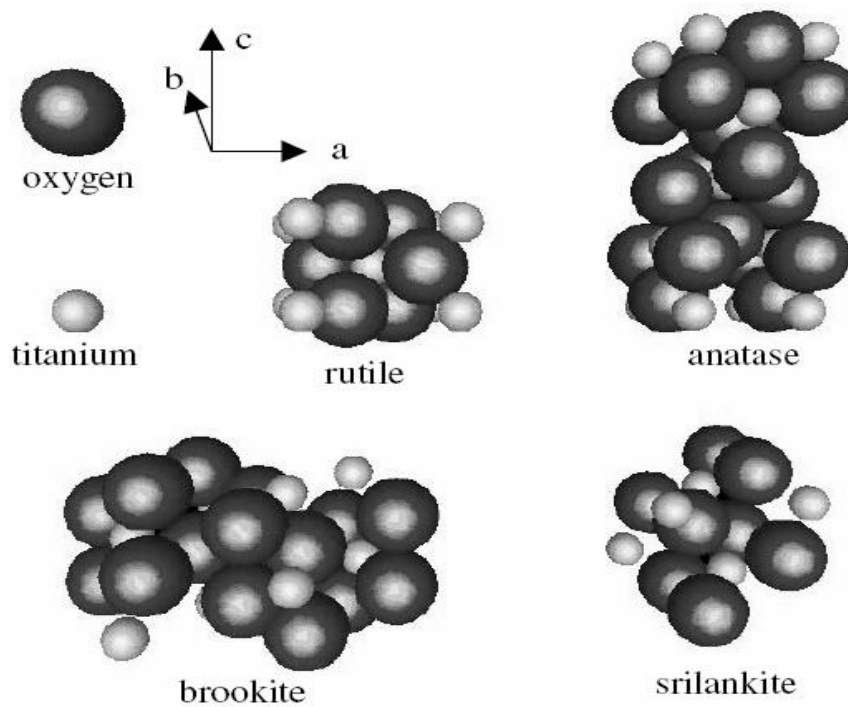
The titanium oxide can crystallize in different structures. At ambient conditions, four structures are known: rutile, anatase, brookite, and srilankite [1]. At higher pressure, i.e. more than 10 Gpa, a baddeleyite structure appears [2], and theoretical work predicts a new structure, not yet observed, similar to fluorite  $HfO_2$  at even higher pressure [3]. The most common and studied structure is rutile, it is also the most stable structure of  $TiO_2$  [4].  $TiO_2$  thin films with all of the four structures can be synthesized, though generally only anatase and rutile are present. The brookite structure has been obtained by the sol-gel method [5-6], and  $TiO_2$ -II (srilankite) has been grown by atomic layer epitaxy from  $TiCl_4$  and  $H_2O$  [7].

Structural, optical, and electrical properties of  $TiO_2$  are reported in (Fig 4.1)

The elementary cells of the  $TiO_2$  crystal structures are presented in (Fig 4.2) Rutile and anatase, which are tetragonal, are more ordered than the orthorhombic structure. The anatase, which is the least dense structure, has empty channels along the a and b axes.

Rutile can exist at any temperature below  $1800^\circ C$ , at which point titanium dioxide becomes liquid, while for temperatures above  $700^\circ C$  the anatase structure changes to the rutile structure [16]. the reverse transformation never occurs. The transformation temperature can be modified by adding impurities into  $TiO_2$ . For instance, the anatase phase completely disappears at temperature of about  $530^\circ C$ ,  $680^\circ C$ , and  $830^\circ C$  for powder samples containing vanadium, molybdenum, and tungsten respectively [17].

polymorph	rutile	anatase	brookite	Srilankite
structure [1]	tetragonal P4 <sub>2</sub> /mnm	tetragonal I4 <sub>1</sub> /amd	orthorhombic Pcab	orthorhombic Pbcn
density [1]	4.25	3.89	4.12	4.37
refraction index $\lambda = 600 \text{ nm}$ [8]	$\perp$ to c axis 2.60 // to c axis 2.89	$\perp$ to c axis 2.55 // to c axis 2.48	// to a or b axis 2.57 // to c axis 2.69	
dielectric constant [9-11]	$\perp$ to c axis 89 // to c axis 173	$\perp$ to c axis 31 // to c axis 48	78	
band gap [eV] [12-13]	$\perp$ to c axis direct 3.04 // to c axis indirect 3.05	$\perp$ to c axis direct 3.42 // to c axis indirect 3.46	3.14	
electron mobility [10 <sup>-4</sup> m <sup>2</sup> /Vs] [12, 14, 15]	crystal: 0.1–10 thin film: 0.1	crystal: 15–550 thin film: 0.1-4		

Figure 4.1:  $TiO_2$  properties.Figure 4.2: Elementary cell of  $TiO_2$  polymorphs

## 4.2 Semiconductor properties

The information given in this section relies on the work of S. M. Sze [18]. Solid materials are classified in three groups depending on their electrical conductivity  $\sigma$ . Highly conducting materials are metals ( $\sigma > 10^4 S m^{-1}$ ), material with very low electrical conductivity are insulators ( $\sigma < 10 - 8 S m^{-1}$ ), and in-between stand the semiconductors. The main difference between metal and

semiconductor is the fact that for metals, the electrical conductivity decreases when temperature increases, while the reverse phenomenon usually occurs in the case of semiconductors.

The energy band diagram of a pure semiconductor containing a negligible amount of impurities (intrinsic semiconductor), is characterized by an energy gap (EG) inside which no electronic states are encountered. The electrical conductivity is given by the following formulas:

$$\sigma = \sigma_n + \sigma_p = q\mu_n n + q\mu_p p$$

Where  $n = N_c \exp\left(-\frac{E_C - E_F}{kT}\right)$  is the electron density in the conduction band

$p = N_v \exp\left(-\frac{E_F - E_V}{kT}\right)$  is the hole density in the valence band

$E_F = \frac{E_C + E_V}{2} + \frac{kT}{2} \ln\left(\frac{N_v}{N_c}\right)$  is the fermi energy

$q$  is the electronic charge,  $k$  is Boltzmann's constant,  $T$  the absolute temperature,  $\mu_n$  and  $\mu_p$  are the electron and hole mobility respectively,  $N_c$  and  $N_v$  are the effective density of state of the conduction and valence band,  $E_C$  the energy of the bottom of conduction band, and  $E_V$  the energy of the top of valence band (see Fig 4.3).

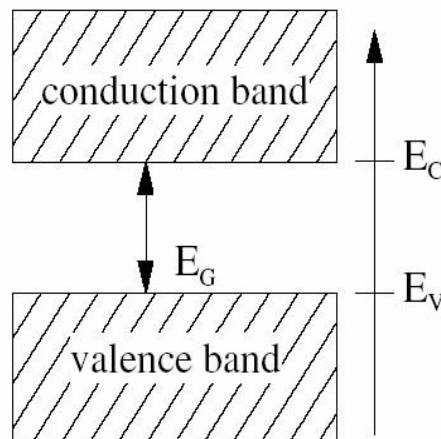


Figure 4.3: Simplified band diagram of a semiconductor

When a semiconductor is doped with donor and/or acceptor impurities, impurity energy levels are introduced. A donor level is defined as being neutral if filled with an electron, and positive if empty. An acceptor level is neutral if empty, and negative if filled by an electron.

The Fermi level for the intrinsic semiconductor lies close to the middle of the bandgap (see Figure 5.3 (a)). When impurity atoms are introduced, the Fermi level must adjust itself to preserve charge neutrality (see Figure 5.3 (b) and (c)), the total negative charge (electrons and ionized acceptors) must equal the total positive charge (holes and ionized donors). n-type (donors impurities) and p-type (acceptor impurities) semiconductor band diagrams and density of states are given in (Fig 4.4) (b) and (c).

Consider the case where donor impurities with concentration  $N_D$  and acceptor impurities with concentration  $N_A$ : the charge neutrality is given by:

$$N_A^- + n = N_D^+ + p$$

Where  $N_D^+ = N_D \left( 1 - \frac{1}{1 + \frac{1}{g_D} \exp\left(\frac{E_D - E_F}{kT}\right)} \right)$  is the number of ionized donors

$$N_A^- = \frac{N_A}{1 + g_A \exp\left(\frac{E_A - E_F}{kT}\right)}$$
 is the number of ionized acceptors

$E_D$  and  $E_A$  the ionization energy of the donors and acceptors, and  $g_D$  and  $g_A$  are the ground-state degeneracies of the donors and acceptors. For a set of given  $N_C$ ,  $N_V$ ,  $N_D$ ,  $N_A$ ,  $E_C$ ,  $E_V$ ,  $E_D$ ,  $E_A$ , and  $T$ , the Fermi level  $E_F$  can be uniquely determined. If  $\mu n$  and  $\mu p$  are known, the electrical conductivity can be calculated.

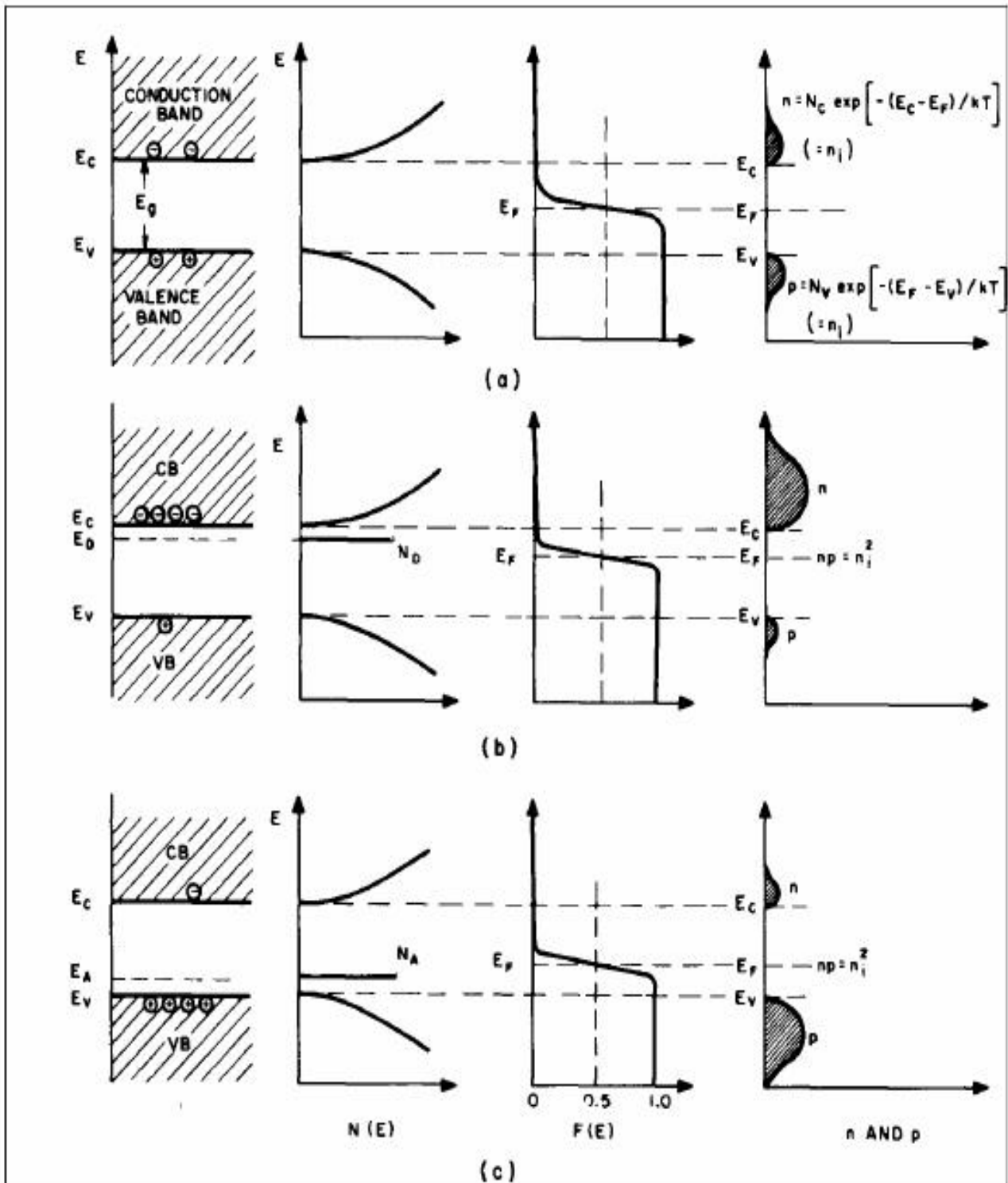


Figure 4.4: Schematic band diagram, density of states, Fermi-Dirac distribution, and the carrier concentration for (a) intrinsic, (b) n-type, and (c) p-type semiconductors at thermal equilibrium [19]

### 4.3 References of Chapter 4

- [1] Standard CPDS X-Ray Diffraction spectra database.
- [2] J. Staun Olsen, L. Gerwald, and J. Z. Jiang, *Journal of Physics and Chemistry of Solids* 60 (1999), 229.
- [3] J. K. Dewhurst and J. E. Lowther, *Physical Review B* 54 (1996), R3673.
- [4] J. Haines and J. N. Leger, *Physica B* 192 (1993), 233.
- [5] Md. Mosaddeq-ur-Rahman, T. Miki, K. Murali Krishna, T. Soga, K. Igarashi, S. Tanemura, and M. Umeno, *Materials Science and Engineering B* 41 (1996), 67.
- [6] M. Gotic, M. Ivanda, A. Sekulic, S. Music, S. Popovic, A. Turkovic, and K. Furic, *Materials Letters* 28(1996), 225.
- [7] J. Aarik, A. Aidla, V. Sammelselg, H. Siimon, and T. Uustare, *Journal of Crystal Growth* 169 (1996), 496.
- [8] J. D'Ans, P. Ten Bruggengate, A. Eucken, G. Joos, and W. A. Roth, *Landolt-Bornstein* 6 II/8, SpringerVerlag, Berlin (1965), 2-145.
- [9] A. Eucken and A. Bchner, *Zeitschrift fr physikalische Chemie B* 27 (1935), 321.
- [10] S. Roberts, *Physical Review* 76 (1949), 1215.
- [11] J. D'Ans, A. Eucken, G. Joos, and W. A. Roth, *Landolt-Bornstein* 6 II/6, Springer Verlag, Berlin (1959), 483.
- [12] H. Tang: "Electronic properties of anatase TiO<sub>2</sub> investigated by electrical and optical measurements on single crystals and thin films", Th EPFL N 1311, Lausanne (1994).
- [13] M. Gratzel and F. P. Rotzinger, *Chemical Physics Letters* 118 (1985), 474.
- [14] L. Forro, O. Chauvet, D. Emin, L. Zuppiroli, H. Berger, and F. Levy, *Journal of Applied Physics* 75 (1994), 633.
- [15] R. G. Breckenridge and W. Hosler, *Physical Review* 91 (1953), 793.
- [16] J. B. Goodenough, A. Hammett, G. Huber, F. Hulliger, M. Leiss, S. K. Ramasesha, and H. Werheit, *Landolt-Bornstein* III/17g, Springer Verlag, Berlin (1984).
- [17] F. Bregani, C. Casale, L. E. Depero, I. Natali-Sora, D. Robba, L. Sangaletti, and G. P. Toledo, *Sensors and Actuators B* 31 (1996), 25.
- [18] S. M. Sze: "Physics of Semiconductor devices", Wiley Interscience, New York (1981).
- [19] S. M. Sze: "Physics of Semiconductor devices", Wiley

Interscience, New York (1981).

# Chapter 5

## Experimental

In this part we describe different step following in the goal to realise Dye-Sensitized Solar Cells which have been made in PMCN laboratory at Lyon 1 University (France). Then the measurements have been made for characterising this cell.

### 5.1 preparation

#### 5.1.1 Components of DSSC

DSSC consist of two glass substrates,each of them coated with a transparent conducting oxide (i.e.  $S_nO_2:F$ ).

On one side of the cell,the photoelectrode,a porous  $TiO_2$  layer composed of nanometer-sized particles. These particles are interconnected to form a three-dimensional nanoporous network. A monolayer of sensitizing dye is adsorbed on the porous  $TiO_2$  film. A monolayer of catalytic platinum is sprayed and serves as the counter-electrode. In a complete cell,the photoelectrode and the counter-electrode are put together,sealed with hot-melt polymer or glue,and the space between the electrodes and the voids between the  $TiO_2$  particles are filled with an electrolyte. [1]

Basically, $TiO_2$ ,dye,electrolyte and Pt catalyst are the most important components in a DSSC. They determine the efficiency and the stability of the DSSC. (Fig 5.1) shows the basic construction of the DSSC.

#### 5.1.2 Materials

TCO Substrates

$TiO_2$  paste made with  $TiO_2$  (P-25, Degussa) which had brought back from EPFL (Lausanne), Laboratory : photopic and interface

$H_2PtCl_6$  solution

N719 dye

Electrolyte ( A6141 type )

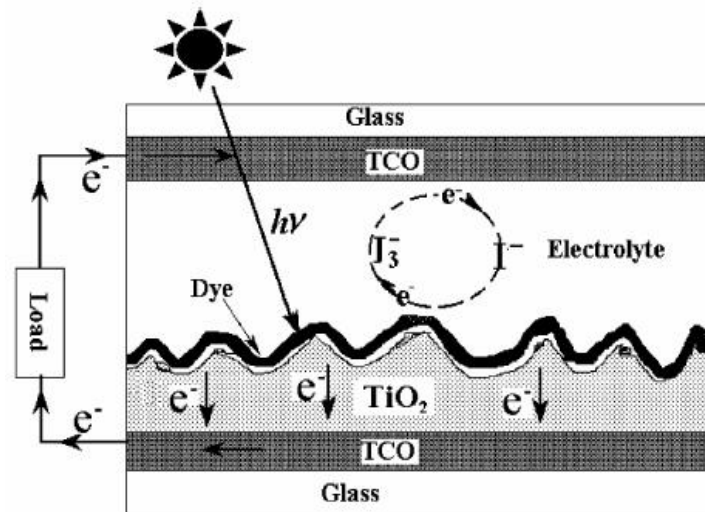


Figure 5.1: The basic construction of a DSSC

### 5.1.3 TCO Substrates

Coated glass with highly F-doped transparent conducting oxide (TCO) usually serves as a support for the dye-sensitized oxide. It allows light transmission while providing good conductivity for current collection. TCO should establish a good mechanical and electrical contact with the dye-sensitized oxide in order to increase electron injection from the latter to the outer circuit.[2]

### 5.1.4 Choice of the TCO

An effective TCO should have high electrical conductivity combined with low absorption of the visible light. However, the decrease of resistivity is correlated with a decreased transmission for a given material. Correspondingly the two parameters have to be optimised for the application of interest. In particular for device used without compact  $TiO_2$  layer the interfacial and material-compatibility properties of the TCO are also important, determining the attachment of the deposited material to the TCO. The TCO should pass the demanding processing conditions for the device preparation without change of its physical properties. The resistance of TCOs will increase, if heated to high temperatures and for long time. However, the TCO typically remains stable up to temperatures slightly above the optimised deposition temperature. Fluorine doped  $S_nO_2$  films are generally very stable, so that the softening of the glass substrate is more limiting than any thermal decomposition of the conducting

layer.[3]

### 5.1.5 Deposited of $TiO_2$ electrodes

Titanium dioxide is widely used as semiconductor material in dye-sensitized nanocrystalline solar cells, owing to its favorable energetics stability, low price and simple processing [4,5].

In the method of preparation of titanium dioxide films electrode, the doctor blade technique shows more fascinating and efficient. It is a simple process leading to films with controllable thickness and surface and more photoactivity [6,7]. The size of the particles and pores making up the film is controlled by the size of the particles in the colloidal solution [8]. The  $TiO_2$  layer is deposited using doctor blade technique as follow :

we crossed a square on scotch then we stucked the scotch on substrate. The paste was deposited onto the substrates and was then spread out using a blade. The thickness of the deposited layer is determined by the Scotch and its dimensions is determined by the square which have been removed. Following spreading, the film was left to dry in air at 80° C for a few minutes and calcined at 500° C for 1h under oxygen .

### 5.1.6 ruthenium sensitizer

The dye is the photoactive element of the photovoltaic device, harvesting the incident light for the photon-to-electron conversion.

One of the most popular sensitizers is the ruthenium dye known as N719, i.e.,  $2(n-C_4H_9)_4N^+$ ,  $[Ru(Hdcbpy)_2(NCS)_2] \cdot 2(H_2dcbpy1/4L1/42, 20-bipyridine-4, 40-dicarboxylic acid)$ , due to its high efficiency and stability [8-9]. Its molecular structure is depicted in (Fig 5.2).

The porous  $TiO_2$  electrodes was immersed in an ethanol solution of a ruthenium-complex (N719) over night for dye-adsorption [10].

### 5.1.7 Preparation of counter Pt-electrodes

To prepare the counter electrode, the FTO glass was washed with  $H_2O$  as well as with ethanol and cleaned by ultrasound in an acetone bath for 10 min. After removing residual organic contaminants by heating in air for 15 min at 400° C,

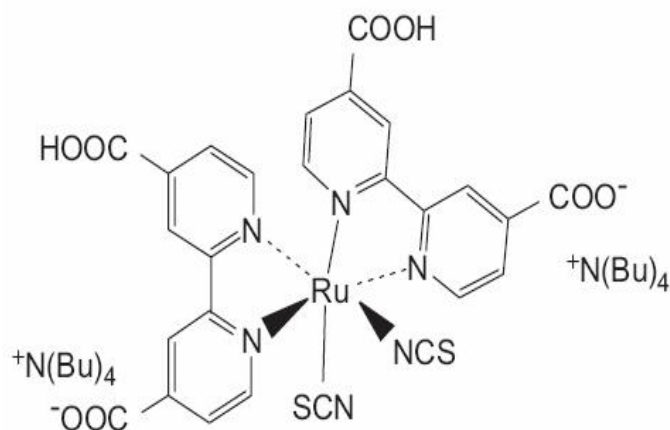


Figure 5.2: Molecular structure of N719

the Pt catalyst was deposited on the FTO glass by coating with a drop of  $H_2PtCl_6$  solution (2 mg Pt in 1 ml ethanol) with repetition of the heat treatment at 400° C for 15 min.[11]

### 5.1.8 Electrolyte

The electrolyte employed was of type A6141 which had brought back from EPFL. but unfortunately the amount was not enough which influenced on the final results.

### 5.1.9 DSSC assemblage

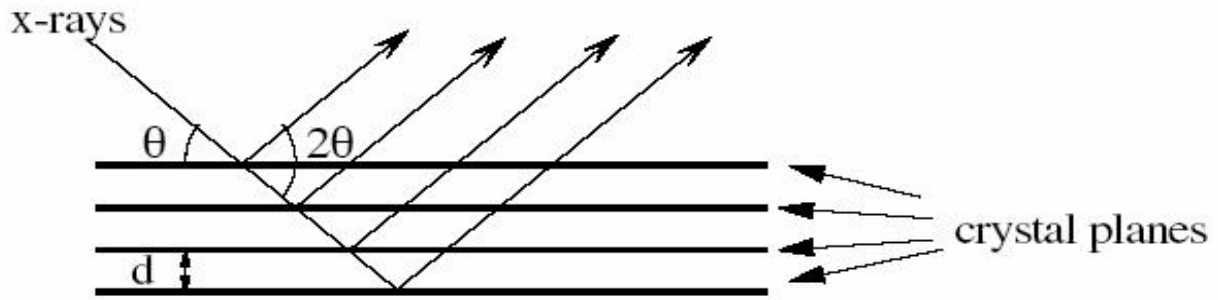
After adding the electrolyte at the dye-covered  $TiO_2$  electrode, it was assembled with Pt-counter electrode into a sandwich type cell. and sealed with a transparency scotch .

In order to have a good electrical contact for the connections to the measurement set-up, the edge of the FTO outside of the cell was sealed with gold plates .

## 5.2 Characterizations methods

### 5.2.1 X-Ray Diffraction

This technique uses the diffraction of x-rays by core electron of atoms. If the sample is a crystal, x-rays are diffracted only in directions verifying the Bragg condition:



where  $d$  is the distance between crystal planes, the incidence angle,  $n$  an integer, and the wavelength of the x-rays.

In the case of our samples, which are polycrystalline thin films, measurements were made with a monochromatic x-ray beam. The diffraction angle  $2\theta$  was varied in an appropriate range and the diffracted intensity was recorded as a function of  $2\theta$ . In principle, each crystal has its own signature: the position of the peaks depends on the crystal symmetry and on the size of the elementary cell of the lattice. Crystalline phases present in a sample can be identified by comparison with X-Ray Diffraction curves compiled in standard databases [12].

The shape of each Bragg peak results from a convolution of the crystallite size, of the experimental resolution function, and of internal stress. If we assume that stress is weak and if the resolution of the setup is good enough, the size can be calculated from the full width at half maximum (FWHM) of the peak with the Scherrer equation [13]:

$$Size = \frac{0.9\lambda}{width \cos \beta} \iff \lambda = 1,54 \text{ \AA}$$

where  $width = \sqrt{FWMH^2 - GW^2}$  in radian, and  $GW$  is the diffractometer broadening.

In mixed anatase-rutile  $TiO_2$  thin films, the weight fraction  $W_a$  of the anatase phase was estimated from the relation:

$$W_a = \frac{1}{1 + 1.265 \frac{I_R}{I_A}}$$

proposed by Spurr [14], where  $I_R/I_A$  is the ratio between the most intense rutile peak ((110),  $2\theta = 27.438^\circ$ ) and the most intense anatase peak ((101),  $2\theta = 25.281^\circ$ ).

### 5.2.2 Photovoltaic characterisation

The two widely used techniques for photovoltaic characterisations are, current-voltage measurements under simulated sunlight and monochromatic light generated current measurements, IPCE.

#### Current-voltage measurements

The dye-sensitised solar cell device can be represented by an equivalent electric scheme shown in (Fig 5.3) [15-17].

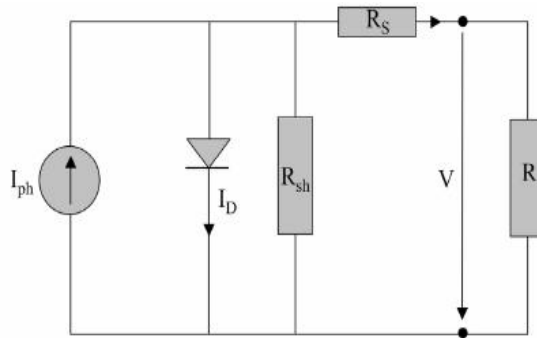


Figure 5.3: Equivalent electric scheme of the dye-sensitised cell

Where  $I_{ph}$  is the photo current,  $I_D$  the diode current,  $R_s$  the series resistance (describes the resistances of the materials) and  $R_{sh}$  the shunt resistance. The equation for the equivalent electric scheme in (Fig 5.3) is:

$$I = I_{ph} - I_s \left[ \exp\left(\frac{V + IR_s}{\eta V_{th}}\right) \right] - \frac{V + IR_s}{R_{sh}} \quad (5.1)$$

The shunt resistance is normally much larger than the series resistance. For this reason one can simplify Equation 6.2:

$$I = I_{ph} - I_s \left[ \exp\left(\frac{V + IR_s}{\eta V_{th}}\right) \right] \quad (5.2)$$

During the current-voltage measurements the following parameter will be determined:

### Short-circuit current ( $I_{sc}$ )

The current equals the short-circuit current when the applied bias potential is zero:

$$I = I_{ph} - I_s \left[ \exp\left(\frac{I_{sc} R_s}{\eta V_{th}}\right) \right] \quad (5.3)$$

When no current is flowing through the cell the potential equals the open-circuit potential, using equation 6.4 one can find:

### Open-circuit potential ( $V_{oc}$ )

$$V_{oc} = \eta V_{th} \ln \left( \frac{I_{ph}}{I_s} + 1 \right) \quad (5.4)$$

### Maximal power output ( $P_{max}$ )

The power delivered from a solar cell at a certain potential equals the product of the current at this potential times the potential:

$$P(V) = I(V) \cdot V \quad (5.5)$$

To obtain a graphic representation of the power one has to vary the potential between  $V_{oc}$  and 0:

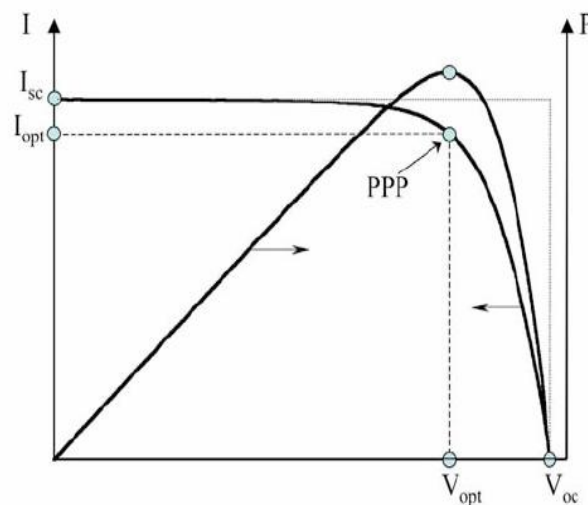


Figure 5.4: Representation of the I/V and the power curves. PPP is the point of peak power

The point where the power is maximum (Pmax) corresponds to the so-called peak power point (PPP) for the I/V curve. These are the optimal current and potential conditions (Iopt, Vopt) for the operating cell. [18].

### Fill-factor (FF)

The fill-factor quantifies the quality of the solar cell, it is obtained by dividing the product of current and voltage measured at the power point by the product of short-circuit current and the open-circuit voltage, as shown in (Fig 5.4): The power point is the maximum product of the cell voltage and the photocurrent obtained on the I-V plot.[19]

$$FF = \frac{I_{mpp} \times V_{mpp}}{I_{sc} \times V_{oc}} \quad (5.6)$$

### Power Conversion Efficiency

The overall conversion efficiency ( $\eta$ ) of the Dye-Sensitized Solar Cell is determined by Equation (6.7). where  $V_{OC}$  is the open circuit voltage,  $I_{sc}$  is the short-circuit current, FF is the fill factor and  $P_{in}$  is the incident light power density, which is standardized at  $1000 \text{ W/m}^2$  for solar cell testing with a spectral intensity distribution matching that of the sun on the earth's surface at an incident angle of  $48.2^\circ$ , which is called the AM 1.5 spectrum [19].

$$\eta_e = \frac{V_{oc} \times I_{sc} \times FF}{P_{in}} \quad (5.7)$$

### Incident Photon-to-current Efficiency

The incident monochromatic photon-to-current conversion efficiency (IPCE), also called external quantum efficiency, is defined as the number of electrons generated by light in the external circuit divided by the number of incident photons as a function of excitation wavelength. It is expressed in Equation (6.8).[20]

$$IPCE = \frac{(1.125 \times 10^3) \times \text{photocurrent density}[mA cm^{-2}]}{\text{wavelength}[nm] \times \text{photoflux}[W m^{-2}]} \quad (5.8)$$

In most cases, the photoaction spectrum overlaps with the absorption spectrum of the sensitizer adsorbed on the semiconductor surface. A high IPCE is

a prerequisite for highpower photovoltaic applications, which depends on the sensitizer photon absorption, excited state electron injection, and electron.

## 5.3 Results and discussion

### 5.3.1 X-Ray Diffraction

The crystalline phase composition of titanium dioxide films electrode was analyzed by X-Ray Diffraction (XRD) which is shown in (Fig 5.5).

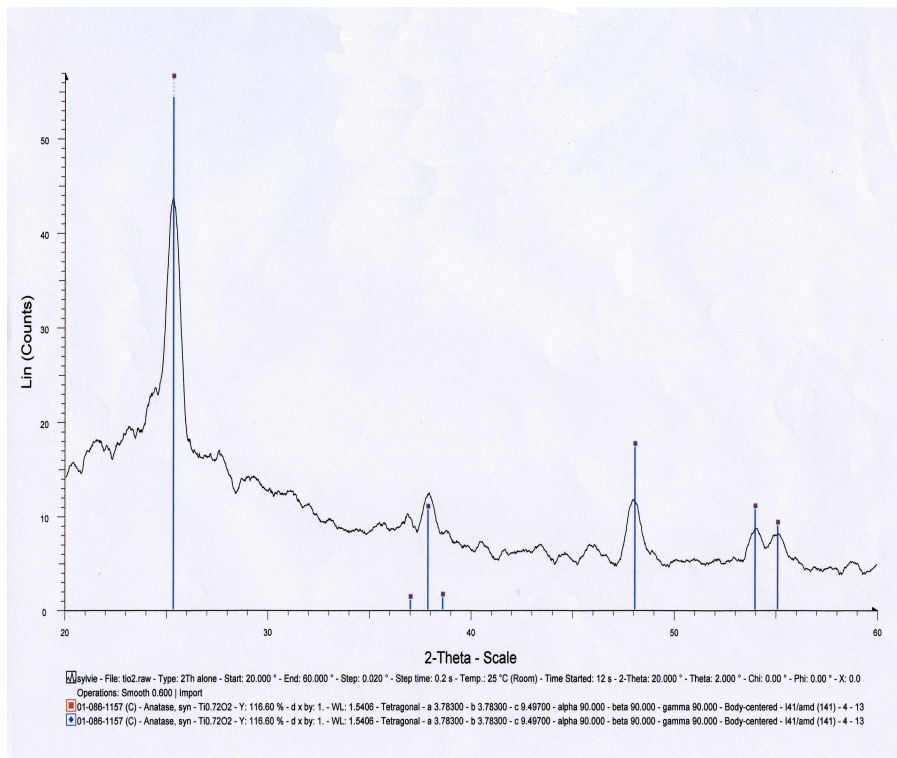


Figure 5.5: X-Ray Diffraction of titanium dioxide films

The most distinctive peaks corresponded to anatase phase . The results obtained from the X-Ray Diffraction clearly reflects that the titanium dioxide films is predominantly composed of anatase .

### 5.3.2 current-voltage measurements

The irradiation source for the photocurrent-voltage (I-V) measurement is a 100 W lamp. The current-voltage curve was obtained by measuring the photocurrent of the cell using an Operator's Manual (Keithley Model 237 Source Measure Units) under an applied external potential scan.

the measurements have been made at physical laboratory of Setif university, (Fig 5.6) shows the Photocurrent density-voltage curve of a cell and (Fig 5.7) shows Power curve of a cell.

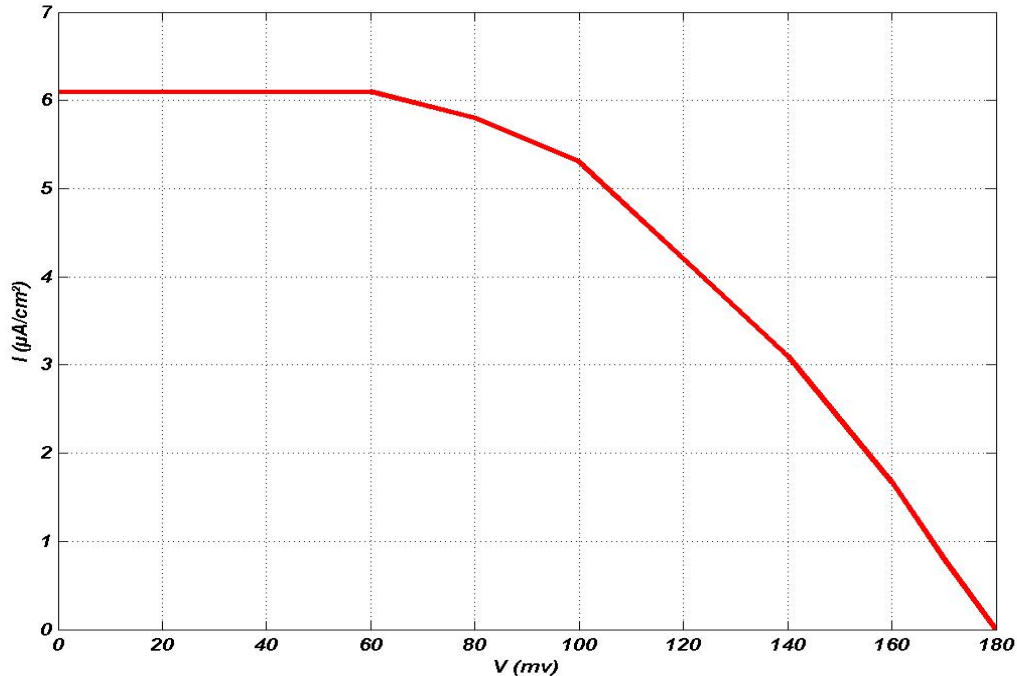


Figure 5.6: Photocurrent density-voltage curve of a cell

I(V) curve shows that the cell functions with  $V_{OC}=180$  mV and  $I_{sc}=6.1$  uA ,which are small values in compare with those reached for this type of cell. These results is explained by the low rate of electron regeneration by the electrolyte due to insufficient amount of the electrolyte used ,and bad sticking of both electrode of the cell have influenced on electron movement in the  $TiO_2$  layer to the back contact (percolation).

The power curve of the cell is drawn using I(V) curve data .

### 5.3.3 The measurement of incident photon-to-current conversion efficiency (IPCE)

The measurement of incident photon-to-current conversion efficiency (IPCE) was performed by a similar data collecting system but under a monochromatic light. IPCE was plotted as a function of excitation wavelength.

The incident light from a 300 W xenon lamp was focused through a Gemini-180 double monochromator onto the cell under test.

The IPCE curve is shown in (Fig 5.8).

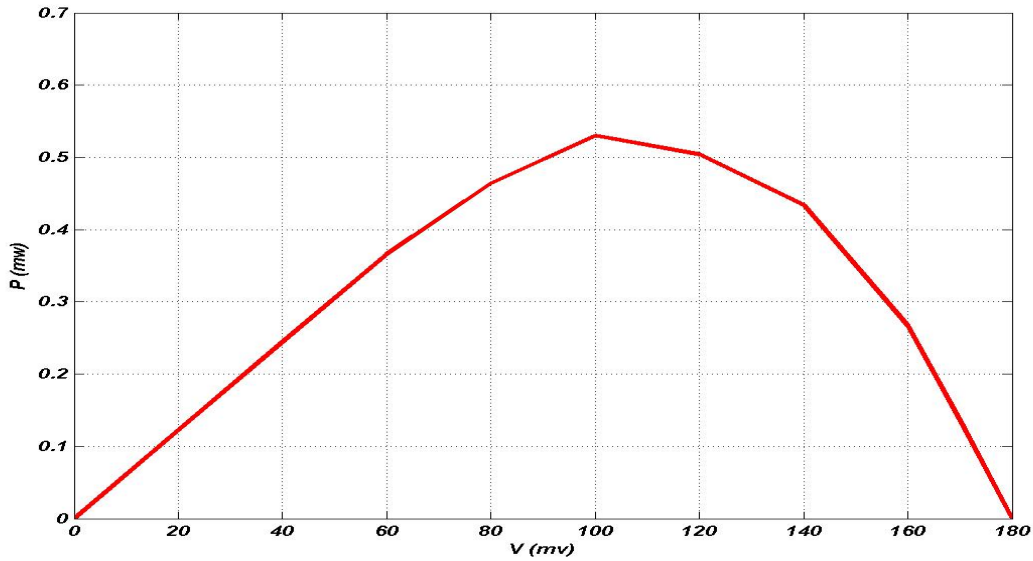


Figure 5.7: Power curve of a cell

Measurements of the power delivered by the cell according to the tension gave us the curve (5.7). It is noticed that the shape of the curve is similar to that which one finds in documentation, but with values very small and a maximum of 0.5mW which is due to the conditions of the manufacture of the cell which is artisanal and to the means used for carried out this cell especially for the stage of the injection of the electrolyte which evaporates after some moment of its injection.

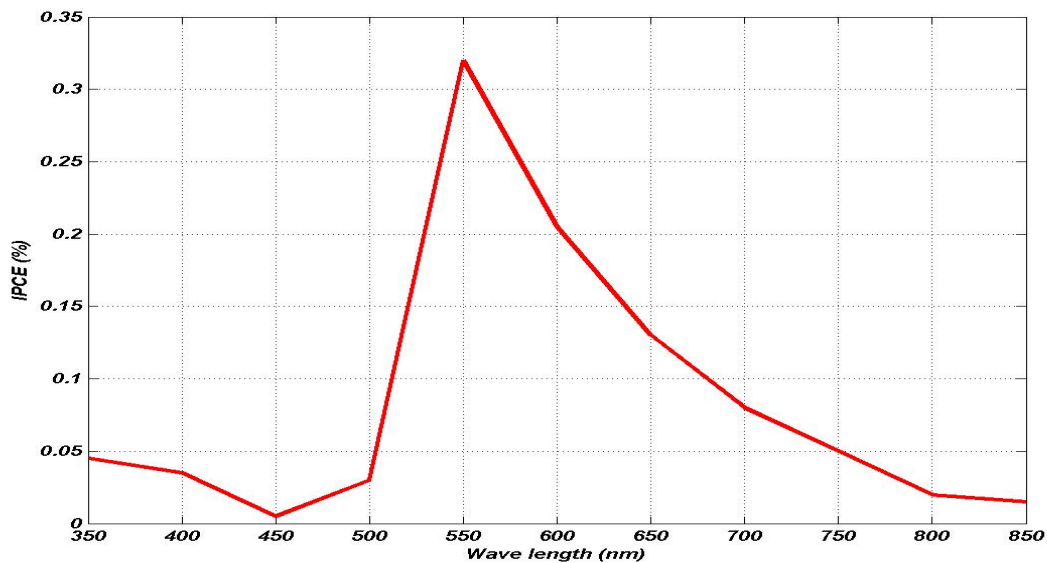


Figure 5.8: IPCE curve of a cell

The measurement of IPCE of the cell gave us a typical curve of the cell when

we see a spade with the value of 550 (wave length) which follows by a degradation of the value until (800 wavelin ght) these resultes is because of initially to the influence of the field of absorption of the dye used on the absorption of light for the cell and still electron transfer which is expressed by the value of IPCE.

The photocurrent action spectrum displays spectral response covering almost the entire visible spectrum, with a peak incident photon-to-current quantum efficiency (IPCE) of approximately 0.32% at a 550 nm incident wavelength.

The short-circuit photocurrent density ( $I_{sc}$ ), open-circuit voltage ( $V_{OC}$ ), fill factor (FF) and solar-to-electricity conversion efficiency ( $\eta$ ) of the cells are summarized in Table (Tab 5.1)

$J_{sc}(\mu A/cm^2)$	$V_{OC}(mV)$	FF	$\eta$	$P_m(mW)$	$I_{pm}(\mu A)$	$V_{pm}(mV)$
6,1	180	0,48	0,017	0,53	5,3	100

Table 5.1: Characteristics of the Cell

Table 5.1 summarizes in general the values which characterize the cell carried out. The value of the output is estimated at 0.017% which is very can compared to the output of the standard cell in the same way, and that is due initially to the condition of realization.

Especially the making of contact which influences negatively transfers from the electrons in the cell and on the power delivered.

## 5.4 References of Chapter 5

- [1] Songyuan Dai\*, Jian Weng, Yifeng Sui, Chengwu Shi, Yang Huang, Shuanhong Chen, Xu Pan, Xiqin Fang, Linhua Hu, Fantai Kong, Kongjia Wang.; *Solar Energy Materials & Solar Cells* 84 (2004) 125-133
- [2] HervUSBAUMER THE N 2955 (2004) Lausanne, EPFL
- [3] Jessica KRER THE N 2793 (2003) Lausanne, EPFL
- [4] G. Boschloo, D. Fitzmaurice, *J. Phys. Chem.* 103 (1999) 2228.
- [5] R.L. Willis, C. Olson, B. O'Regan, et al., *J. Phys. Chem. B* 106 (2002) 7605.
- [6] A. Hagfeldt, M. Gratzel, *Acc. Chem. Res.* 33 (2000) 267.
- [7] K.J. Jiang, T. Kitamura, H. Yin, S. Ito, *Chem. Lett.* 9 (2002) 872.
- [8] M.K. Nazzerruddin, A. Kay, I. Podicio, R. Humphry-Baker, E. M. uller, P. Liska, N. Vlachopoulos, M. Gratzel, *J. Am. Chem. Soc.* 115 (1993) 6382.
- [9] M.K. Nazeeruddin, A. Kay, I. Rodicio, R. Humphry-Baker, E. Muller, P. Liska, P.N. Vlachopoulos, M. Gratzel, *J. Am. Chem. Soc.* 115 (1993) 6382.
- [10] B. O'Regan, M. Gratzel, *Nature* 353 (1991) 737.
- [11] Seigo Ito, Takurou N. Murakami, Pascal Comte, Paul Liska, Carole Gratzel, Mohammad K. Nazeeruddin, Michael Gratzel. .2007.05.090
- [12] Standard CPDS X-Ray Diffraction spectra database.
- [13] P. Scherrer, *Gott. Nachr* 2 (1918), 98.
- [14] R. A. Spurr, and H. Myer, *Analytical Chemistry* 29 (1957), 760.
- [15] Ricaud, A. *Photopiles solaires*; Presses polytechniques et universitaires romandes: Lausanne, 1997.
- [16] Planta, C. v. *Die photoelektrische Charakterisierung der mit Farbstoff sensibilisierten nanokristallinen Solarzellen*, EPFL, 1996.
- [17] Krueger, J. *Interface engineering in solid-state dye-sensitized solar cells*, EPFL, 2003.
- [18] H. Hoppe, N.S. Sariciftci, *J. Mater. Res. Soc.* 19 (2004) 7.
- [19] J. Rotalsky, D. Meissner, *Sol. Energ. Mat. Sol. Cells* 63 (2000)
- [20] 2003 MD. K. Nazeeruddin and M. Gratzel. Published by Elsevier Ltd.

# CONCLUSIONS

The objective of this work was to study and to realise a relatively new class of low-cost solar cell, that belong to the group of thin-film solar cells which known as dye-sensitized solar cell (DSSC). In this work, we have illustrated the working principle of the dye-sensitized solar cell and details of its components. Then a cell of this type was realised. The crystalline phase composition of titanium dioxide films electrode was analyzed by X-ray diffraction (XRD). the dye-sensitized solar cell realized in this work was characterised with The standard characterization techniques of DSSC include the currentvoltage measurements under simulated sunlight and monochromatic light generated current measurements, IPCE. We have measured the current density-voltage (J-V) characteristics of a cell which have given the Photocurrent density-voltage curve and Power curve of a cell. The measurement of incident photon-to-current conversion efficiency (IPCE) was made for obtaining the IPCE curve of a cell. The short-circuit current density ( $J_{sc}$ ), open-circuit voltage ( $V_{oc}$ ), fill factor (ff) and power conversion efficiency ( $\eta$ ) of cell was given.